Top-quark pair production in association with a $W^{\pm}$ gauge boson in the POWHEG-BOX

F. Febres Cordero[*], M. Kraus[†], and L. Reina[‡]

Physics Department, Florida State University, Tallahassee, Florida 32306-4350, USA

We present a new Monte Carlo event generator for the production of a top-quark pair in association with a $W^{\pm}$ boson at hadron colliders in the POWHEG-BOX framework. We consider the next-to-leading-order QCD corrections to the $pp \to t\bar{t}W^{\pm}$ cross section, corresponding to the $\mathcal{O}(\alpha_s^3 \alpha)$ and $\mathcal{O}(\alpha_s \alpha^3)$ terms in the perturbative expansion of the parton-level cross section, and model the decays of W and top quarks at leading order retaining spin correlations. The fixed-order QCD calculation is further interfaced with the PYTHIA8 parton-shower event generator via the POWHEG method as implemented in the POWHEG-BOX. The corresponding code is now part of the public repository of the POWHEG-BOX. We perform a comparison of different event generators for both the case of inclusive production and the case of the two same-sign leptons signature at the Large Hadron Collider operating at a center-of-mass energy of 13 TeV. We investigate theoretical uncertainties in the modeling of the fiducial volume stemming from missing higher-order corrections, the different parton-shower-matching schemes, and the modeling of decays. We find that the subleading contribution at $\mathcal{O}(\alpha_s \alpha^3)$ is particularly sensitive to differences in the matching scheme and higher-order parton-shower effects. We observe that in particular jet observables can differ quite visibly although these differences play only a subordinate role in the description of physical observables once all contributions are combined.

I. INTRODUCTION

The production of top-quark pairs in association with electroweak gauge bosons (W, Z, γ) can be measured at the Large Hadron Collider (LHC) and future hadron colliders (HL-LHC, FCC-hh, and CppC) in a multitude of decay channels and provides new avenues to test the consistency of the Standard Model (SM) in processes that have been beyond the energy reach of existing colliders or statistically limited until recently. At the same time, these processes represent some of the most important backgrounds for Higgs-boson precision measurements and searches of new physics beyond the Standard Model (BSM). In this context, the hadronic production of $W^{\pm}$ bosons in association with top-quark pairs is particularly interesting both from a phenomenological and a theoretical point of view.

On top of its intrinsic interest as a SM process, $t\bar{t}W^{\pm}$ provides very distinctively polarized top quarks that can be used to unveil the imprint of new physics interactions. Indeed, in contrast to top-quark pair production, the top quarks originating from the $t\bar{t}W^{\pm}$ production process are highly polarized and give rise to a large $t\bar{t}$ charge asymmetry [1,2]. A measurement of the $t\bar{t}$ charge asymmetry in $t\bar{t}W^{\pm}$ production can then be sensitive to the chiral nature of new physics contributing to the process and can become a unique indirect probe of BSM physics.

The $t\bar{t}W^{\pm}$ processes also represent a very important background to the production of a Higgs boson in association with top quarks in the multilepton decay channels [3–7], where it limits the accuracy of the direct measurement of the top-quark Yukawa coupling. In addition, $t\bar{t}W^{\pm}$ is the dominant background in searches for the SM production of four top quarks [8,9]. In general, $t\bar{t}W^{\pm}$ is a background to any search of new physics in signatures with same-sign leptons, missing energy, and b jets, common in many BSM models.

Due to its phenomenological relevance, the process has been studied extensively on the theory side, starting from the first calculation of next-to-leading-order (NLO) QCD corrections to the production and decay process in Ref. [10]. Further studies at fixed order include the calculation of the leading NLO electroweak (EW) corrections [11] and the assessment of the impact of formally subleading mixed QCD and EW corrections [12]. Beyond fixed order the pure NLO QCD $t\bar{t}W^{\pm}$ calculation has been

[*]ffebres@hep.fsu.edu
[†]mkraus@hep.fsu.edu
[‡]reina@hep.fsu.edu

matched to parton showers using the POWHEG method [13,14] as implemented in the PowHel framework [15] as well as using the MC@NLO method [16,17] in the MG5_aMC@NLO framework [1].[1] Separately, the resummation of soft gluon emission effects have been studied at the next-to-next-to-leading logarithmic accuracy [25–29].

On the experimental side, the associate $t\bar{t}W^{\pm}$ production has been measured by the LHC experiments both as inclusive cross section [30,31] and as a background in searches for $t\bar{t}H$ and $t\bar{t}t\bar{t}$ signals [6–9] in multilepton decay channels. Some of these measurements have resulted in larger values with respect to SM predictions. Because of this, the modeling of the $t\bar{t}W^{\pm}$ processes has come under more thorough scrutiny, with the recent inclusion of off-shell and nonresonant effects at fixed-order NLO QCD [32,33] and by studying the effect of spin correlations and formally subleading EW corrections in the fiducial volume of specific $t\bar{t}W^{\pm}$ signatures [34]. Also, estimates of the impact of higher-order QCD corrections beyond NLO corrections, estimated via multijet merging, on inclusive $t\bar{t}W^{\pm}$ samples, has been presented in Ref. [35]. Furthermore, the ATLAS Collaboration recently performed a dedicated comparison of the implementation of $t\bar{t}W^{\pm}$ production in existing NLO parton-shower Monte Carlo event generators, including both QCD and EW effects and allowing for multijet merging [36].

In this paper we continue the investigation of modeling uncertainties of the $t\bar{t}W^{\pm}$ process, by presenting a study based on a new implementation of the $pp \to t\bar{t}W^{\pm}$ production in the POWHEG-BOX framework [37]. We consider next-to-leading-order QCD corrections to the $pp \to t\bar{t}W^{\pm}$ cross section, corresponding to the $\mathcal{O}(\alpha_s^3\alpha)$ and $\mathcal{O}(\alpha_s\alpha^3)$ terms in the perturbative expansion of the parton-level cross section, and model the decays of W and top quarks at leading order (LO) retaining spin correlations.

As part of our study, we perform a detailed comparison between different NLO parton-shower Monte Carlo event generators at both the inclusive and the fiducial level in order to address modeling uncertainties. We compare results obtained with our POWHEG-BOX implementation (interfaced to the PYTHIA8 [38,39] parton shower), with Sherpa (using its parton shower based on Catani-Seymour dipoles [40]), and with MG5_aMC@NLO (also interfaced to PYTHIA8) and present a first study of the consistency between these different frameworks. Our comparison provides a solid basis on which to develop a more robust estimate of the residual theoretical uncertainty and suggests

which aspects of the theoretical prediction for hadronic $t\bar{t}W^{\pm}$ production still need improvement.

The paper is organized as follows. In Sec. II we review the POWHEG method to the extent of allowing us to establish our notation. In Sec. III we provide details of our implementation of the $t\bar{t}W^{\pm}$ processes in the POWHEG-BOX framework. In Sec. IV we present theoretical predictions for both inclusive $t\bar{t}W^{\pm}$ production and for a two same-sign leptons signature, comparing results from different Monte Carlo event generators. Finally, we give our summary and outlook in Sec. V.

II. REVIEW OF THE POWHEG FRAMEWORK

Matching parton-shower Monte Carlo event generators with fixed-order perturbative calculations to achieve NLO accuracy for inclusive observables has proven fundamental to describe LHC data. Two major strategies for this *matching* are commonly employed, the MC@NLO [16,17] and POWHEG [13,14] methods. In this article we employ the latter using the POWHEG-BOX framework [37] to study event simulation associated to $t\bar{t}W^{\pm}$ production at hadron colliders.

Within the POWHEG method the matching of NLO matrix elements to parton showers is achieved by generating the hardest emission first with NLO QCD accuracy, while subsequent emissions are modeled by the parton shower. Starting with the NLO fixed-order cross section

$$\sigma^{\text{NLO}} = \int d\Phi_n[B(\Phi_n) + V(\Phi_n)] + \int d\Phi_{n+1}R(\Phi_{n+1}), \quad (1)$$

where $d\Phi_n$ denotes the n-particle Lorentz-invariant phase space measure and $B(\Phi_n)$, $V(\Phi_n)$, and $R(\Phi_{n+1})$ are the differential Born, virtual, and real cross sections, respectively, one introduces a *jet function* $F(\Phi_{n+1})$ to split the real radiation contribution as

$$R(\Phi_{n+1}) = F(\Phi_{n+1})R(\Phi_{n+1}) + [1 - F(\Phi_{n+1})]R(\Phi_{n+1}) \quad (2)$$

and uses it to define the *soft* $R_s(\Phi_{n+1})$ and *hard* $R_h(\Phi_{n+1})$ real contributions according to

$$R_s(\Phi_{n+1}) \equiv F(\Phi_{n+1})R(\Phi_{n+1}),$$
$$R_h(\Phi_{n+1}) \equiv [1 - F(\Phi_{n+1})]R(\Phi_{n+1}). \quad (3)$$

The jet function $F(\Phi_{n+1})$ is a real function which takes values between 0 and 1 and should approach smoothly 1 in the infrared (soft and collinear) limits of the $(n+1)$-particle phase space Φ_{n+1}. The precise functional form of $F(\Phi_{n+1})$ is in principle arbitrary, but a judicious choice is in certain cases necessary to avoid large matching corrections, which are formally subleading. Below we discuss standard choices made in the POWHEG-BOX, and in Sec. IV we will study their impact on the process at hand.

---

[1]A comparison of $t\bar{t}W^{\pm}$ differential distributions obtained from MG5_aMC@NLO [18], PowHel [15] and Sherpa [19,20] + OpenLoops [21–23] including $\mathcal{O}(\alpha_s^3\alpha)$ NLO QCD corrections has been presented in Ref. [24] as a validation of the corresponding Monte Carlo tools. Reference [24] also provided LHC $t\bar{t}W^{\pm}$ cross sections for $\sqrt{s} = 13$ and 14 TeV including $\mathcal{O}(\alpha_s^3\alpha)$ and $\mathcal{O}(\alpha_s^2\alpha^2)$ NLO corrections as obtained from both MG5_aMC@NLO and Sherpa + OpenLoops.

To generate the first (hardest) emission while keeping the NLO accuracy for inclusive observables, a one-step parton shower is introduced according to

$$
\sigma^{\text{NLO+PS}} = \int d\Phi_n \bar{B}(\Phi_n) \left[\Delta(\Phi_n, p_T^{\text{min}}) \right.
$$
$$
+ \int d\Phi_r \frac{R_s(\Phi_{n+1})}{B(\Phi_n)} \Delta(\Phi_n, p_T) \left. \right]
$$
$$
+ \int d\Phi_{n+1} R_h(\Phi_{n+1}), \qquad (4)
$$

where the real emission phase space is factorized as $d\Phi_{n+1} = d\Phi_n d\Phi_r$ in terms of the underlying Born phase space with n final-state particles ($d\Phi_n$) and the phase space of the radiated particle ($d\Phi_r$), the $\bar{B}(\Phi_n)$ function is defined by

$$
\bar{B}(\Phi_n) \equiv B(\Phi_n) + V(\Phi_n) + \int d\Phi_r R_s(\Phi_{n+1}), \quad (5)
$$

and we have introduced the modified Sudakov form factor $\Delta(\Phi_n, p_T)$, which is defined as

$$
\Delta(\Phi_n, p_T)
$$
$$
= \exp\left(-\int d\Phi_r \frac{R_s(\Phi_n, \Phi_r)}{B(\Phi_n)} \Theta(k_T(\Phi_n, \Phi_r) - p_T) \right). \quad (6)
$$

In Eq. (4) the parton-shower infrared cutoff scale is denoted with p_T^{min} and $p_T = p_T(\Phi_r)$ is the transverse momentum of the emitted particle.

The modified Sudakov form factor ensures that no double counting of real radiation in R_s is produced, while radiation from R_h is treated as an independent contribution. This highlights the importance of the choice of $F(\Phi_{n+1})$ for the POWHEG method. As already mentioned, after the first (hardest) emission, subsequent splittings can be generated by a standard parton shower without affecting the NLO accuracy for inclusive observables.

In the POWHEG-BOX the function $F(\Phi_{n+1})$ is written as the product of two functions [37,41] according to

$$
F(\Phi_{n+1}) = F_{\text{damp}}(\Phi_{n+1}) F_{\text{bornzero}}(\Phi_{n+1}), \qquad (7)
$$

where by default $F_{\text{damp}}(\Phi_{n+1})$ and $F_{\text{bornzero}}(\Phi_{n+1})$ are set identical to 1, such that $F(\Phi_{n+1}) = 1$ and consequently $R_s = R$ and $R_h = 0$. When enabling a nontrivial F_{damp} in the POWHEG-BOX, the corresponding function takes the form

$$
F_{\text{damp}}(\Phi_{n+1}) = \frac{h_{\text{damp}}^2}{h_{\text{damp}}^2 + p_T^2}, \qquad (8)
$$

where h_{damp} is a dimensionful parameter that can either be set to a constant value or to a function of the underlying

Born kinematics Φ_n. The function F_{damp} then ensures that events with large p_T are treated as part of the hard real contributions R_h, while events in soft and collinear regions (where $p_T \rightarrow 0$) are associated to R_s.

On the other hand, when enabling a nontrivial F_{bornzero}, the corresponding function takes the form [37,42]

$$
F_{\text{bornzero}}(\Phi_{n+1}) = \Theta\left(h_{\text{bornzero}} - \frac{R(\Phi_{n+1})}{P_{ij}(\Phi_r) \otimes B(\Phi_n)} \right), \quad (9)
$$

where $P_{ij}(\Phi_r) \otimes B(\Phi_n)$ is an approximation to $R(\Phi_{n+1})$ based on the factorization properties of the real amplitudes in the soft and collinear limits. The dimensionless parameter h_{bornzero} controls how much phase space outside of the singular limits is associated to R_s.[2] In particular, it ensures that if $B(\Phi_n)$ vanishes in certain regions of phase space, no large contributions from the first term on the right-hand side of Eq. (4) will be produced. While historically this was the main reason to introduce F_{bornzero}, this function also helps to identify and distinguish different enhancement mechanisms of the real matrix elements, which should not be interpreted as due to QCD splittings. As we will see, this plays a crucial role for the $\mathcal{O}(\alpha_s \alpha^3)$ contributions in our present study.

As a final remark, we would like to highlight that the role played by the POWHEG damping functions is different from the role played by the initial shower scale μ_Q in the MC@NLO method. In the POWHEG method the damping functions are used to control the degree of resummation for nonsingular contributions, while the initial shower scale is always assigned by the POWHEG framework to be the transverse momentum of the parton splitting independent of whether that splitting is associated to R_s, the *soft*, or to R_h, the *hard* contribution. Thus, the function $F(\Phi_{n+1}) = F_{\text{damp}}(\Phi_{n+1}) F_{\text{bornzero}}(\Phi_{n+1})$ can have a substantial impact on the generated event sample but only a mild impact on the subsequent parton-shower evolution. In contrary, the initial shower scale μ_Q of the MC@NLO method directly controls the available phase space for subsequent parton-shower emissions and therefore can have a strong impact on the shower evolution. The impact of the damping function and the initial shower scale is formally of higher order and does not spoil the NLO accuracy of the predictions. Nonetheless, these higher-order corrections can become sizable.

III. DETAILS OF THE CALCULATION

In this section we present our implementation of the $pp \rightarrow t\bar{t}W^{\pm}$ process in the POWHEG-BOX including NLO corrections. We start by discussing the perturbative orders in $\alpha_s^n \alpha^k$ that we are considering.

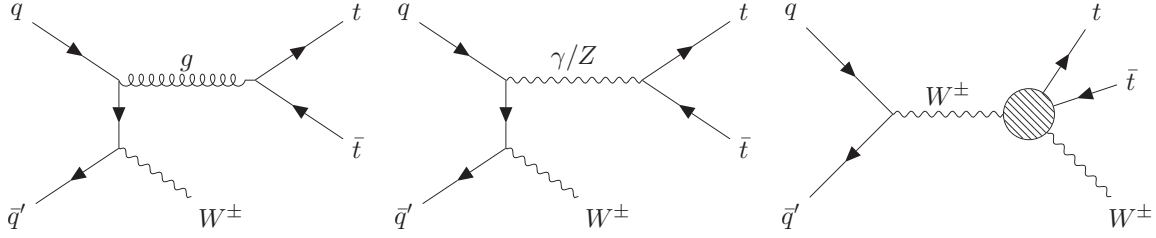[2]The default value of h_{bornzero} is 5 in the POWHEG-BOX.

FIG. 1.   Representative Feynman diagrams for QCD (left) and EW (middle and right) tree-level contributions to the $pp \to t\bar{t}W^{\pm}$ process. Contributions to the $WWtt$ blob on the right are shown in Fig. 2.
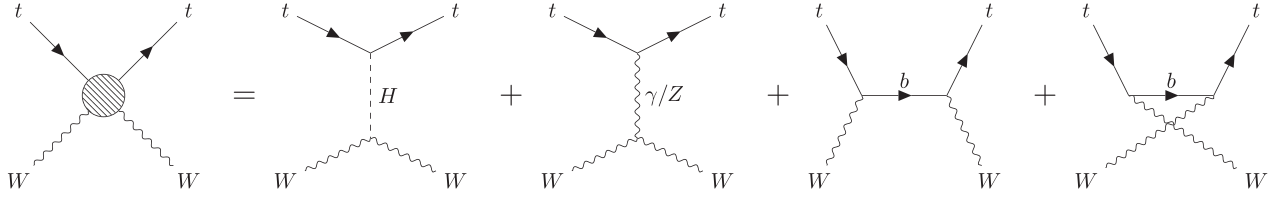

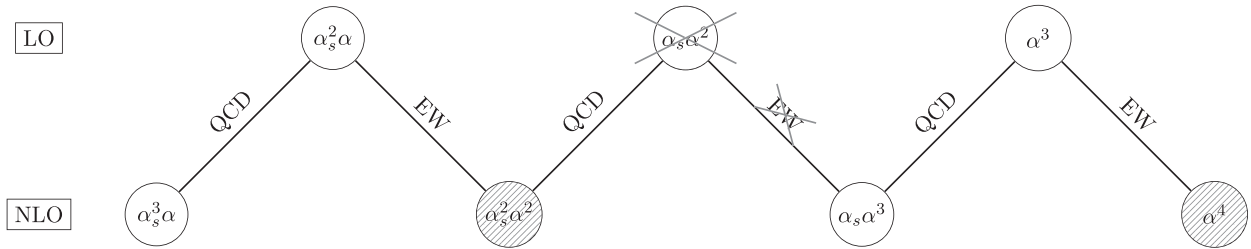FIG. 2.   The diagrams contributing to the $WWtt$ tree-level amplitude in unitary gauge.

FIG. 3.   The possible coupling combinations contributing to the LO and NLO $t\bar{t}W^{\pm}$ cross section. The links indicate how a given NLO order originates from a corresponding LO order via QCD or EW corrections. The terms crossed out vanish by color structure. In this study the orders corresponding to the shaded bubbles are neglected.

At tree level the $t\bar{t}W^{\pm}$ final state can be generated in hadron collisions via $q\bar{q}' \to t\bar{t}W^{\pm}$ subprocesses, as illustrated in Fig. 1. As illustrated in Fig. 3 the corresponding LO cross section receives contributions from three different coupling combinations, namely $\mathcal{O}(\alpha_s^2\alpha)$, $\mathcal{O}(\alpha_s\alpha^2)$, and $\mathcal{O}(\alpha^3)$, although the QCD-EW interference term of $\mathcal{O}(\alpha_s\alpha^2)$ vanishes by color structure (as indicated in Fig. 3 by having it crossed out). At the next order in the QCD or EW couplings all four orders illustrated in the second line of Fig. 3 are generated. At this level, the classification into pure QCD or EW corrections generally breaks down since the two kinds of corrections start to mix. For example terms of order $\mathcal{O}(\alpha_s^2\alpha^2)$ can be interpreted as QCD corrections to the $\mathcal{O}(\alpha_s\alpha^2)$ or as EW corrections to the $\mathcal{O}(\alpha_s^2\alpha)$ LO cross section. In general, in the presence of mixed NLO corrections the complexity of these computations increases substantially, as infrared QED and QCD singularities have to be subtracted simultaneously. At the same time, a proper matching to a parton-shower Monte Carlo event generator would have to consider both QCD and QED radiation in the parton shower.

In the case of $t\bar{t}W^{\pm}$, the identification in terms of QCD and EW corrections can be restored to a very good approximation by considering the hierarchy of the different leading and subleading orders of the NLO cross section. As shown in Refs. [12,43], apart from the dominant $\mathcal{O}(\alpha_s^3\alpha)$ term which amounts to about 50% of the LO cross section (at $\sqrt{s} = 13$ TeV), among all other subleading contributions the $\mathcal{O}(\alpha_s\alpha^3)$ is surprisingly the most relevant, amounting to about 10% of the LO cross section. In comparison the $\mathcal{O}(\alpha_s^2\alpha^2)$ represents only about 4% of the LO cross sections and the $\mathcal{O}(\alpha^4)$ is below per mille level.[3]

---

[3]Incidentally, notice that the $\mathcal{O}(\alpha_s^2\alpha^2)$ and $\mathcal{O}(\alpha^4)$ NLO corrections include photon-initiated contributions of the form $q\gamma \to t\bar{t}W^{\pm}q'$ which however amount to a small fraction of these already subleading corrections [11].
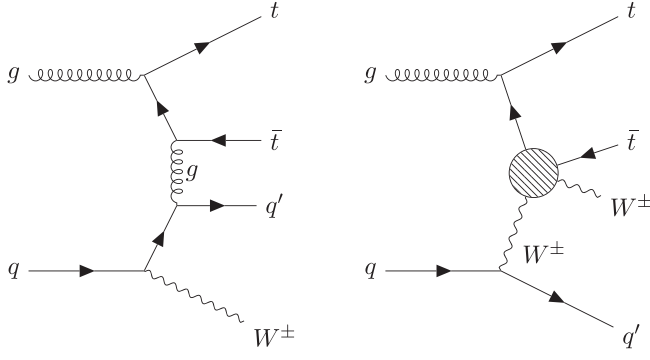
FIG. 4. Representative Feynman diagrams for the new gq channel that opens up at NLO and that contributes at $\mathcal{O}(\alpha_s^3\alpha)$ (lhs) and $\mathcal{O}(\alpha_s\alpha^3)$ (rhs). Contributions to the $WWtt$ blob on the right are shown in Fig. 2.

The enhancement of the $\mathcal{O}(\alpha_s\alpha^3)$ terms originates from NLO QCD real corrections from the qg channel that opens at NLO QCD and, more specifically, from the kind represented by the right-hand side diagram in Fig. 4. In these particular contributions, the parton density enhancement of qg versus $q\bar{q}$ is largely amplified by the combined effect of several factors, from the t-channel kinematic to the rescattering of W and Z longitudinal components, and the presence of a large top-quark Yukawa coupling.

Being able to consider only the *leading* $\mathcal{O}(\alpha_s^3\alpha)$ and $\mathcal{O}(\alpha_s\alpha^3)$ NLO contributions allows one to unambiguously interpret them as NLO QCD corrections to the $\mathcal{O}(\alpha_s^2\alpha)$ and the $\mathcal{O}(\alpha^3)$ LO cross sections, respectively. Indeed, the $\mathcal{O}(\alpha_s\alpha^3)$ terms can only arise from QCD corrections to the $\mathcal{O}(\alpha^3)$ LO since EW corrections to the $\mathcal{O}(\alpha_s\alpha^2)$ LO interference term vanish by color structure (see Fig. 3). As such, the fixed-order NLO QCD calculation can be consistently interfaced with a QCD parton-shower event generator.

In the following we will then focus solely on the contributions at the perturbative orders $\mathcal{O}(\alpha_s^2\alpha)$ and $\mathcal{O}(\alpha_s^3\alpha)$, which we will denote from now on as "$t\bar{t}W^{\pm}$ QCD," and the orders $\mathcal{O}(\alpha^3)$ and $\mathcal{O}(\alpha_s\alpha^3)$, which we will denote as "$t\bar{t}W^{\pm}$ EW." Results from our implementation of $pp \to t\bar{t}W^{\pm}$ in the POWHEG-BOX have the same level of theoretical accuracy as the ones presented in Ref. [34] and can be directly compared to the ones that can be obtained via analogous NLO QCD parton-shower Monte Carlo event generators such as Sherpa or MG5_aMC@NLO + PYTHIA8. Indeed, we will show a corresponding comparison among these tools in Sec. IV.

Next, we will discuss in Sec. III A the implementation of $pp \to t\bar{t}W^{\pm}$ including the aforementioned orders of NLO QCD corrections in the POWHEG-BOX framework. Furthermore, in Sec. III B we will give some further details on the modeling of a fully realistic final state by including decays of unstable particles while keeping spin correlations at LO accuracy.

A. NLO corrections to the production of $t\bar{t}W^{\pm}$

The implementation of a new process in the POWHEG-BOX requires to provide process-specific ingredients such as the LO and NLO virtual and real matrix elements as well as the parametrization of the Born-level phase space, while all process-independent parts, such as the subtraction of infrared singularities, are automated. In our implementation of $t\bar{t}W^{\pm}$, all tree-level matrix elements including spin- and color-correlated Born matrix elements are taken from the MadGraph4 [44,45] interface that is provided within the POWHEG-BOX. The finite remainders of the virtual loop corrections interfered with the Born matrix elements are computed by the fairly new one-loop provider for QCD and EW corrections NLOX [46,47] that uses OneLOop [48] for the evaluation of scalar Feynman integrals. The parametrization of the $t\bar{t}W^{\pm}$ phase space has been directly modeled on the POWHEG-BOX implementation of $t\bar{t}H$ [49].

We performed several checks to validate our implementation. For example, virtual amplitudes have been successfully compared at a few phase-space points against Recola [50,51] and MadGraph5 [52]. At the same time, total inclusive cross sections at fixed order have been cross-checked with MG5_aMC@NLO [18], while a full validation at the differential level has been performed by comparing to an independent calculation obtained from Sherpa [19,20] in conjunction with either the version of the Blackhat library of Ref. [53] or with the OpenLoops program [21–23].

On the other hand, as explained in Sec. II, in matching the fixed-order calculation with parton-shower event generator within the POWHEG-BOX framework, we have implemented the following choices for the jet function $F(\Phi_{n+1})$ of Eq. (7). First, similar to the case of $b\bar{b}W^{\pm}$ [54], the leading-order matrix element at $\mathcal{O}(\alpha_s^2\alpha)$ has vanishing Born-level configurations. Therefore, the usage of $F_{\text{bornzero}}(\Phi_{n+1})$ [see Eq. (9)] is mandatory for $t\bar{t}W^{\pm}$ QCD production. This is also applied to $t\bar{t}W^{\pm}$ EW production, where it plays a critical role given the presence of the strongly enhanced real matrix element discussed before (due to the diagrams of the right of Fig. 4). Finally we have enabled the damping function $F_{\text{damp}}(\Phi_{n+1})$ of Eq. (8) to further suppress hard radiation using a dynamic value of h_{damp}. More specifically, our default choices for the *damping* parameters will be

$$h_{\text{damp}} = \frac{H_T}{2}, \qquad h_{\text{bornzero}} = 5, \qquad (10)$$

where

$$H_T = \sum_{i \in \{t,\bar{t},W\}} \sqrt{m_i^2 + p_{T,i}^2} \qquad (11)$$

is evaluated on the underlying Born kinematics.

In order to disentangle the impact of the jet function $F(\Phi_{n+1})$ from possible parton-shower corrections, we

investigate the differential distributions of POWHEG-BOX events without taking into account the parton-shower evolution. We show a few representative observables in Fig. 5 at the level of Les Houches events (LHE) [55,56]. On the left we show transverse momentum distributions for the leading jet, the top-quark pair, and the $W^{\pm}$ boson for inclusive $t\bar{t}W^{\pm}$ QCD production, while on the right we show the transverse momentum and pseudorapidity distributions of the leading jet, as well as the transverse momentum distribution of the $W^{\pm}$ boson for inclusive $t\bar{t}W^{\pm}$ EW production. In all cases, we compare POWHEG-BOX predictions with and without the effect of the jet function $F(\Phi_{n+1})$ (labeled as LHE-damping and LHE-no damping, respectively) to the corresponding fixed-order differential distributions.

For inclusive $t\bar{t}W^{\pm}$ QCD production we observe large shape differences between the fixed-order NLO prediction and the POWHEG-BOX results without the jet function. In hadronic observables such as the transverse momentum of the hardest jet the differences reach up to a factor of 3 at a transverse momentum of around 600 GeV. A similar behavior can be seen in the transverse momentum of the top-quark pair, where the deviations are up to +70% at the end of the plotted range. Even in nonhadronic observables such as the transverse momentum of the $W^{\pm}$ boson moderate differences at the level of 10% are visible. However once the damping mechanism is taken into account the predictions recover the tails of the NLO fixed-order distributions, which are reliably described by fixed-order matrix elements. Though considerable improvement is achieved for the transverse momentum distribution of the hardest jet with the inclusion of the jet function, still a small difference of about 10% is observed for large $p_T(j_1)$. On the other hand, shape differences for low p_T values such as in the case of the transverse momentum of the leading jet are attributed to the resummation of soft and collinear QCD splittings via the Sudakov form factor and are thus expected to be different from the fixed-order result. In the case of inclusive $t\bar{t}W^{\pm}$ EW production the impact of the jet function is more dramatic. Here, the NLO QCD corrections are dominated by real radiative contributions that are enhanced by the t-channel EW scattering of $tW \to tW$ shown in Figs. 2 and 4. Therefore, the resummation of the full real matrix element yields unphysical results as nonfactorizing contributions are resummed and thus the jet function $F(\Phi_{n+1})$ has to be used to restrict the resummation to singular QCD splittings that indeed factorize. As a consequence of choosing a trivial jet function $F(\Phi_{n+1}) = 1$, the shapes of the transverse momentum and the rapidity distributions of the leading jet are described poorly over the entire phase space. Also the transverse momentum of the $W^{\pm}$ boson shows large discrepancies in the tail of the distribution. Nonetheless, using our default jet function $F(\Phi_{n+1})$ parameters [see Eq. (10)] we observe an excellent

agreement between the NLO fixed-order computation and the POWHEG-BOX results. Furthermore, the impressive agreement of the transverse momentum distribution of the leading jet down to low values of $p_T(j_1)$ just highlights how radiation attributed to the *hard* contribution R_h [see Eq. (4)] dominates the production of that leading jet, while enhancements from resummation effects are nearly negligible.

B. Decay modeling of the $t\bar{t}W^{\pm}$ system

In order to be able to study a broader range of exclusive observables, which depend strongly on spin correlations from production to decaying particles, we include the decay of the $t\bar{t}W^{\pm}$ system in our implementation. Typically, parton-shower event generators decay unstable particles during the shower evolution. This approach is the simplest but it cannot preserve spin correlations in the decays, as each particle is decayed independently. In the following we briefly discuss our implementation of the decays in the POWHEG-BOX that preserves spin correlations at least to LO accuracy, which can have a sizable impact on the top-quark decay products since the emission of the $W^{\pm}$ boson in the initial state polarizes the top quarks [1,34].

Our approach follows closely the method of Ref. [57]. This method has been adopted in the POWHEG-BOX already for several processes (see for example Refs. [49,54,58,59]). The basic idea can be summarized as follows. Starting from an on-shell phase space point for the $t\bar{t}W^{\pm}$ momenta one performs a reshuffling of the momenta to allow for off-shell virtualities of the unstable particles. Afterward, momenta of decay products are generated uniformly in the decay phase space and finally these momenta are unweighted against the fully decayed matrix element by constructing a suitable upper bounding function.

All previous implementations in the POWHEG-BOX have in common that only the decay of a top-quark pair has been taken into account. In order to allow these reshuffles for more than two unstable particles, we introduce a new momentum mapping in a process-independent and Lorentz-invariant way.

The POWHEG-BOX, after the single-step parton-shower process (see Sec. II), generates on-shell momentum configurations Φ_n^{OS} that either refer to a $t\bar{t}W^{\pm}$ or a $t\bar{t}W^{\pm}j$ final state. We start by generating independent virtualities v^2 for each top quark and $W^{\pm}$ boson according to Breit-Wigner distributions

$$\rho(v^2) = \frac{m_f \Gamma_f}{\pi} \frac{1}{(v^2 - m_f^2)^2 + m_f^2 \Gamma_f^2}, \qquad (12)$$

where m_f and Γ_f are the particle mass and decay width. We constrain the generated virtualities to the window $|v - m_f| < 5\Gamma_f$. These virtualities will be imprinted onto
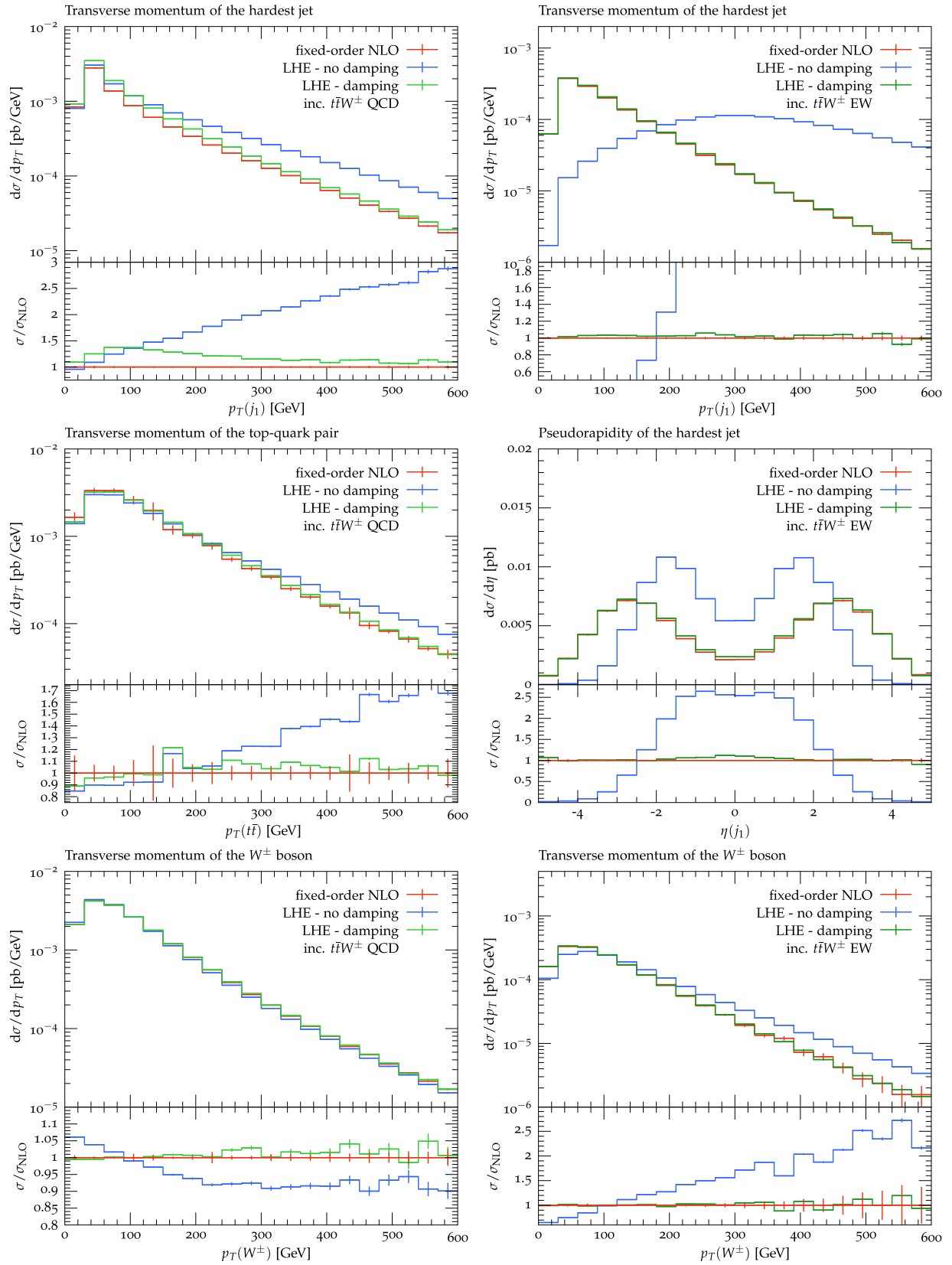
FIG. 5.   Impact of the jet function $F(\Phi_{n+1})$ [see Eq. (7)] on differential distributions. The *LHE-damping* curves correspond to our default choice of parameters according to Eq. (10).

the momenta of the on-shell phase space point Φ_n^{OS} by the repeated application of the mapping presented in the Appendix, where we choose to preserve the momentum of the light jet in the case of a real radiation event. This amounts to choosing $Q = p_t + p_{\bar{t}} + p_W$ as the total available momentum in the mapping of the Appendix and excluding the jet from the Lorentz boost. In the following we will call the off-shell phase space configuration simply Φ_n.

Afterward, momenta of the decay products are uniformly generated as a sequence of $1 \rightarrow 2$ decays. This allows one also to include off-shell W bosons in the top-quark decays. In the last step we apply the *hit-and-miss* technique (see e.g., Ref. [58]) on the so-obtained final-state momenta using an upper bounding function $U_{\text{dec}}(v_t^2, v_{\bar{t}}^2, v_W^2, \Phi_{t \rightarrow b\ell\nu}, \Phi_{\bar{t} \rightarrow \bar{b}\ell\nu}, \Phi_{W \rightarrow \ell\nu})$, constructed according to Ref. [57], such that

$$\frac{\mathcal{M}_{\text{dec}}(\Phi_n, \Phi_{t \rightarrow b\ell\nu}, \Phi_{\bar{t} \rightarrow \bar{b}\ell\nu}, \Phi_{W \rightarrow \ell\nu})}{\mathcal{M}_{\text{undec}}(\Phi_n^{\text{OS}})}$$
$$\leq U_{\text{dec}}(v_t^2, v_{\bar{t}}^2, v_W^2, \Phi_{t \rightarrow b\ell\nu}, \Phi_{\bar{t} \rightarrow \bar{b}\ell\nu}, \Phi_{W \rightarrow \ell\nu}), \quad (13)$$

where $\mathcal{M}_{\text{undec}}(\Phi_n^{\text{OS}})$ is the LO matrix element for the undecayed process, while $\mathcal{M}_{\text{dec}}(\ldots)$ is a so-called decay-chain matrix element, which corresponds to a LO matrix element for the fully decayed process where only diagrams with the resonance structure of interest are kept. These decay-chain matrix elements are taken from MG5_aMC@NLO [18].

The result of this procedure is such that all spin correlations between unstable particles and decay particles are kept with LO precision.

For completeness, we briefly discuss the extension to the $t\bar{t}W^{\pm}$ process of the method to choose particular decay signatures, which has been previously used in POWHEG-BOX implementations. We present details for the $t\bar{t}W^+$ process, as the $t\bar{t}W^-$ process is treated in an analogous way. All top quarks decay into a W boson and a b quark, and we now have to take into account the decay of three W bosons. Based on the branching ratios $\text{Br}(W \rightarrow \ell_i \nu_i)$ and $\text{Br}(W \rightarrow q_i \bar{q}_i')$ we can construct a density matrix ρ for the decay probabilities:

$$\rho_{ijk} = \text{Br}(W^+ \rightarrow X_i)\text{Br}(W^- \rightarrow \bar{X}_j)\text{Br}(W^+ \rightarrow X_k), \quad (14)$$

where $X_i(\bar{X}_i)$ represent the possible (charge conjugated) final states, namely

$$X_1 = e^+\nu_e, X_2 = \mu^+\nu_\mu, X_3 = \tau^+\nu_\tau, X_4 = u\bar{d}, X_5 = c\bar{s}. \quad (15)$$

The total branching ratio is then given by

$$\text{Br}_{\text{tot}} = \sum_{i,j,k} \rho_{ijk}, \quad (16)$$

which can be less than 1 if, for example, only particular decay channels are selected.

To choose a particular decay channel we simply perform a hit-and-miss procedure on the components of the probability density matrix ρ. To allow for hadronic decays we take into account the Cabibbo-Kobayashi-Maskawa (CKM) mixing of the first two generations, which is parametrized by

$$V_{\text{CKM}} = \begin{pmatrix} V_{ud} & V_{us} & V_{ub} \\ V_{cd} & V_{cs} & V_{cb} \\ V_{td} & V_{ts} & V_{tb} \end{pmatrix} = \begin{pmatrix} \cos\theta_c & \sin\theta_c & 0 \\ -\sin\theta_c & \cos\theta_c & 0 \\ 0 & 0 & 1 \end{pmatrix}. \quad (17)$$

For example, when the decay $W^+ \rightarrow u\bar{d}$ has been chosen we simply generate a random number $r \in [0, 1]$ and if $r \leq |V_{us}|^2 = \sin^2\theta_c$, we choose the decay $W^+ \rightarrow u\bar{s}$; otherwise we keep the decay $W^+ \rightarrow u\bar{d}$.

At last we would like to mention that with the procedure outlined above the symmetry factors for identical final-state particles are obtained in the correct way. For example, for a calculation employing full off-shell matrix elements it is clear that

$$\sigma(pp \rightarrow b\bar{b}e^+\nu_e\mu^-\bar{\nu}_\mu e^+\nu_e)$$
$$= \frac{1}{2}\sigma(pp \rightarrow b\bar{b}e^+\nu_e\mu^-\bar{\nu}_\mu\tau^+\nu_\tau), \quad (18)$$

due to symmetry factors. Since in our methodology we generate decays subsequently we have to ensure that the probability to generate the $e^+\mu^-\tau^+$ final state is twice as large as the one for the $e^+\mu^-e^+$ final state. This is trivially ensured in our procedure, since

$$\text{Br}(t\bar{t}W^{\pm} \rightarrow e^+\mu^-e^+) = \rho_{121} = \frac{1}{729} \quad (19)$$

and

$$\text{Br}(t\bar{t}W^{\pm} \rightarrow e^+\mu^-\tau^+) = \rho_{123} + \rho_{321} = \frac{2}{729}, \quad (20)$$

where we have used $\text{Br}(W \rightarrow \ell_i\nu_i) = 1/9$.

We performed several cross-checks on the modeling of the decays. For instance, we checked that the correct branching ratios are obtained from inclusive event samples that take into account all possible decay modes. Also, we compared at the differential level unshowered leading-order events for a particular decay mode with events obtained through the same procedure by MG5_aMC@NLO in conjunction with MadSpin [60] and found perfect agreement.

IV. PHENOMENOLOGICAL RESULTS

In this section we present and discuss numerical results for $pp \rightarrow t\bar{t}W^{\pm}$ obtained with the new POWHEG-BOX

implementation described in this paper and compare them with analogous results obtained from MG5_aMC@NLO and Sherpa. After reviewing the general settings for the input parameters of our study in Sec. IV A, we will consider the case of inclusive $t\bar{t}W^{\pm}$ production in Sec. IV B and the case of a specific signature with two same-sign leptons and jets (usually referred to as $2\ell SS$) in Sec. IV C. In the following we will denote by $t\bar{t}W^{\pm}$ the sum of both $t\bar{t}W^{+}$ and $t\bar{t}W^{-}$ production.

A. Computational setup

In our study we consider $t\bar{t}W^{\pm}$ production at the LHC with a center-of-mass energy of $\sqrt{s} = 13$ TeV. All results presented in this section have been obtained using the NNPDF3.0 [61] (NNPDF30-nlo-as-0118) parton distribution functions (PDFs) as provided by LHAPDF [62]. We have not performed a detailed study of the PDF uncertainty associated with this production mode since it does not directly affect either the comparison between fixed-order and parton-shower results or the comparison between different NLO parton-shower Monte Carlo event generators. Of course such uncertainty should be included in future more comprehensive assessments of the overall theoretical uncertainty on this production mode.

The necessary Standard Model parameters have been chosen to be

$$G_F = 1.166378 \times 10^{-5} \text{ GeV}^{-2}, \qquad m_t = 172.5 \text{ GeV}, \qquad m_b = 0 \text{ GeV},$$
$$M_W = 80.385 \text{ GeV}, \qquad M_Z = 91.1876 \text{ GeV}, \qquad M_H = 125 \text{ GeV},$$
$$\Gamma_t = 1.33247 \text{ GeV}, \qquad \Gamma_W = 2.09767 \text{ GeV}, \qquad \Gamma_Z = 2.50775 \text{ GeV}, \tag{21}$$

in terms of which the electromagnetic coupling is defined as

$$\alpha = \frac{\sqrt{2}}{\pi} G_F M_W^2 \left(1 - \frac{M_W^2}{M_Z^2}\right). \tag{22}$$

The central values of the renormalization and factorization scales are set to

$$\mu_R = \mu_F = \mu_0 = \frac{H_T}{2}, \tag{23}$$

with

$$H_T = \sum_{i \in \text{final state}} \sqrt{m_i^2 + p_{T,i}^2}. \tag{24}$$

The theoretical uncertainties associated with this choice of scales are estimated via the seven-point envelope that corresponds to μ_R and μ_F assuming the following sets of values:

$$\left(\frac{\mu_R}{\mu_0}, \frac{\mu_F}{\mu_0}\right) = \{(0.5, 0.5), (0.5, 1), (1, 0.5),$$
$$(1, 1), (1, 2), (2, 1), (2, 2)\}. \tag{25}$$

We notice that in quoting the dependence of the results presented in this section from scale variation, the previously defined scale variation has been applied only to the hard matrix elements, while scale choices in the parton shower have not been altered.

In order to assess the nature and size of theoretical uncertainties present in the modeling of the $t\bar{t}W^{\pm}$ process,

we will compare results from three different NLO parton-shower event generators, POWHEG-BOX, MG5_aMC@NLO, and Sherpa, using the setups described next. In the following figures we will label the results obtained using different tools accordingly.

(i) POWHEG-BOX.—We generate results using the POWHEG-BOX implementation presented in this paper by performing the parton-shower matching to PYTHIA8 [39] (v. 8.303) using the POWHEG method as described in Secs. II and III A and modeling the decay of the $t\bar{t}W^{\pm}$ final state as discussed in Sec. III B. We employ by default the *damping* parameters shown in Eq. (10), that is

$$h_{\text{damp}} = \frac{H_T}{2}, \qquad h_{\text{bornzero}} = 5,$$

where the dynamic damping parameter h_{damp} is evaluated on the underlying Born kinematics. The impact of different choices of damping parameters is estimated by the five-point envelope that corresponds to choosing the values

$$(h_{\text{damp}}, h_{\text{bornzero}}) = \left\{\left(\frac{H_T}{2}, 5\right), \left(\frac{H_T}{2}, 2\right),\right.$$
$$\left.\left(\frac{H_T}{2}, 10\right), \left(\frac{H_T}{4}, 5\right), (H_T, 5)\right\}. \tag{26}$$

For PYTHIA8 we use the $A14$ shower tune and turn off all its matrix element corrections (MECs) to decay processes.

(ii) MG5_aMC@NLO.—We obtain results using MG5_aMC@NLO (v2.7.2) by performing the parton-shower matching to PYTHIA8 with the MC@NLO method. Here the initial shower scale is set to $\mu_Q = H_T/2$ and decays of unstable particles are taken into account via the MadSpin framework. Also for MG5_aMC@NLO we assess the matching uncertainties related to the initial shower scale by making a three-point envelope which corresponds to the values

$$\mu_Q = \left\{ \frac{H_T}{4}, \frac{H_T}{2}, H_T \right\}. \qquad (27)$$

For PYTHIA8 we use the $A14$ shower tune with the standard MG5_aMC@NLO parameter settings, which also do not include MEC to decay processes.

(iii) Sherpa.—Finally, we use the Sherpa (v2.2.10) parton-shower event generator to produce a third set of independent results. For $t\bar{t}W^\pm$ QCD production we use the MC@NLO matching procedure and Sherpa's parton shower, which is based on Catani-Seymour dipole factorization [40]. The corresponding one-loop matrix elements for these studies are taken from the OpenLoops [21–23] program. To produce predictions with Sherpa's public version for $t\bar{t}W^\pm$ EW production we employed a truncated shower merging procedure (MEPS/CKKW) setup [63,64], including LO matrix elements for the processes $t\bar{t}W^\pm$ and $t\bar{t}W^\pm j$ [at $\mathcal{O}(\alpha^3)$ and $\mathcal{O}(\alpha_s\alpha^3)$, respectively]. The latter setup catches key contributions for $t\bar{t}W^\pm$ EW production, in particular the large hard real contributions. We do not show scale variations or matching uncertainties for Sherpa, as we have checked that variations of its resummation scale produces similar results to those obtained with MG5_aMC@NLO shower scale variations, in agreement with the findings of Ref. [36]. In Sherpa spin-correlated decays are implemented via the method presented in Ref. [65].

We do not include in any of the previous setups non-perturbative corrections like those from hadronization or multiple parton interactions. Notice that, even though the hard NLO computation is performed in a massless five-flavor scheme, the used parton showers in this study adopt by default a nonzero bottom mass.

Combining the effect of renormalization and factorization scale variation with the variations induced by different choices of matching schemes and parton-shower codes enables us to address the numerical impact of higher-order corrections that are inherent to each approach. We want to emphasize however that the variation of damping parameters and the initial shower μ_Q have different effects as explained at the end of Sec. II. Nonetheless, we will refer to the sensitivity of the predictions on these parameters as an *uncertainty.*

The showered events are finally passed via the HepMC [66,67] interface to an analysis routine written in the Rivet framework [68,69].

In Supplemental Material [70] that we make available with this document we provide the necessary files to reproduce our results. They include run cards for POWHEG-BOX and Sherpa as well as our Rivet analyses.

B. Inclusive NLO + PS observables

In this section we study the on-shell inclusive production of $t\bar{t}W^\pm$ and the impact of the parton-shower evolution on inclusive observables. To this end we focus on differential distributions that can also be computed at fixed order and compare the NLO fixed-order results to the corresponding results obtained by parton-shower matching in different frameworks.

For this analysis we keep the top quarks and $W^\pm$ bosons stable. No cuts are applied on the top quarks and $W^\pm$ bosons. Jets are formed using the anti-k_T jet algorithm [71] with a resolution parameter of $R = 0.4$ as implemented in FastJet [72,73]. We require a minimal transverse momentum of $p_T > 25$ GeV for all jets. Note that we do not distinguish between light and b-flavored jets in obtaining the results presented in this section.

In the following we will discuss first the $t\bar{t}W^\pm$ QCD and $t\bar{t}W^\pm$ EW contributions to the $t\bar{t}W^\pm$ inclusive cross section separately, as they show different overall features. Afterward, we will study the impact of the EW contribution on the QCD + EW combined prediction for a few representative observables.

1. $t\bar{t}W^\pm$ QCD contribution

We start our discussion by focusing on the dominant $t\bar{t}W^\pm$ QCD contribution. Figure 6 shows the transverse momentum of the top-quark pair $[p_T(t\bar{t})]$ as well as of the $W^\pm$ boson $[p_T(W^\pm)]$ at fixed order and for various predictions including parton showers. The middle panel depicts the ratio with respect to the fixed-order NLO results and the uncertainty bands correspond to independent variations of renormalization and factorization scales in the hard matrix elements. The bottom panel shows the matching uncertainties as estimated by the variation of damping parameters and the initial shower scale μ_Q, as stated in Sec. IV A, normalized to the fixed-order NLO result.

In the case of the transverse momentum of the top-quark pair all three predictions agree well with the fixed-order NLO prediction over the whole plotted range. The theoretical uncertainties due to scale variation are of the order of 10% at the beginning and grow up to 30% at the end of the spectrum. The matching uncertainties are smaller than the scale uncertainties in the whole plotted range and reach at most 7% in the tail of the distribution. Also for the transverse momentum of the $W^\pm$ boson, predictions agree
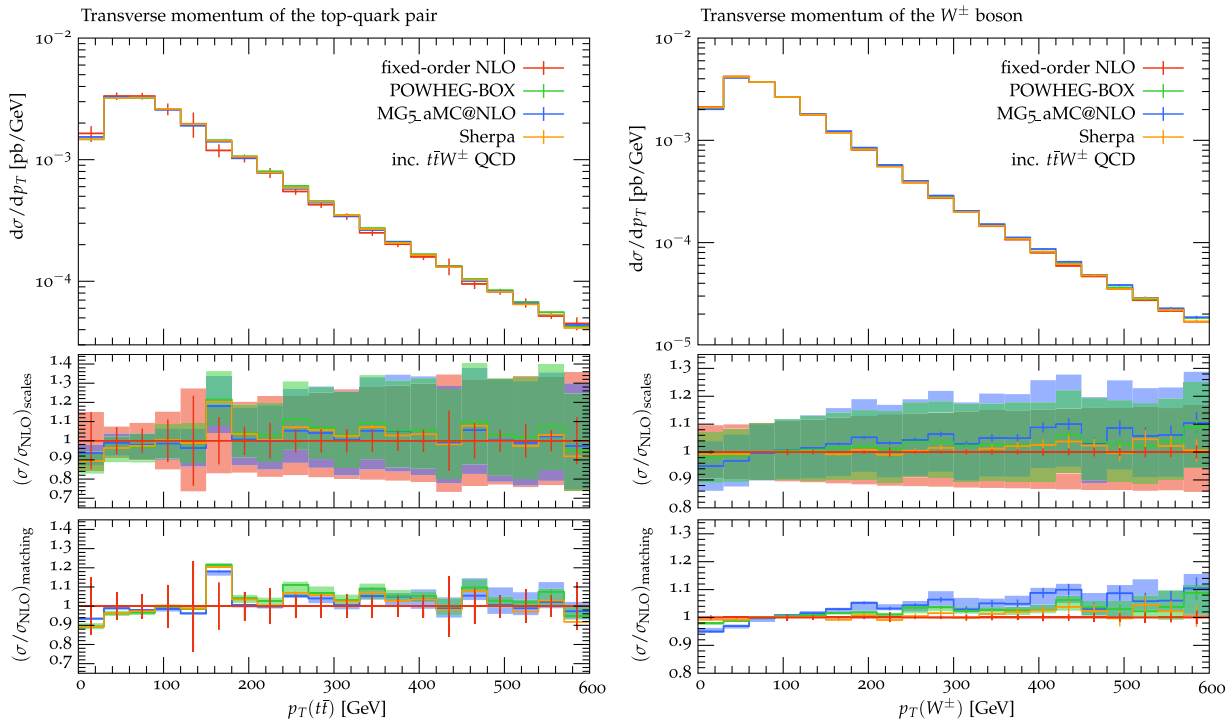
FIG. 6.   Inclusive $t\bar{t}W^{\pm}$ QCD production as a function of the transverse momentum of the top-quark pair (lhs) and of the $W^{\pm}$ boson (rhs) for various event generators. The uncertainty bands (not shown for Sherpa) correspond to independent variations of renormalization and factorization scales (middle panel) and of the matching parameters (bottom panel).

well with the fixed-order result. Only results obtained from MG5_aMC@NLO show a small shape difference with respect to the fixed-order NLO prediction. However, within the estimated theoretical uncertainties of 10%–15%, predictions from all generators considered agree well with each other. Again, the matching uncertainties are small compared to the scale uncertainties, as it is expected for inclusive NLO observables, and are below 5%.

Next we turn to less inclusive observables such as the transverse momentum $[p_T(j_1)]$ and the pseudorapidity $[\eta(j_1)]$ of the hardest jet, as shown in Fig. 7. These observables are only accurate to LO since they do not receive one-loop corrections and can thus be more affected by the parton-shower evolution. For example, in the case of the transverse momentum of the hardest jet, modifications to the spectrum are expected for small transverse momenta due to the Sudakov resummation in the parton shower, while the high-energy tail should be well described by using fixed-order matrix elements. Indeed all predictions including parton-shower effects differ from the fixed-order curve by up to 21%–30% for small transverse momenta, where POWHEG-BOX predictions differ the most. On the other hand, in the high-energy tail of the distribution all event generators recover the fixed-order prediction starting from $p_T \gtrsim 300$ GeV, with POWHEG-BOX showing the best agreement whereas MG5_aMC@NLO and Sherpa give a slightly softer spectrum than the fixed-order curve by roughly 10% at the end of the plotted spectrum. In addition

to the shape differences we also notice a severe reduction of the theoretical uncertainties in the beginning of the spectrum where the parton shower is expected to dominate. While the fixed order has nearly constant uncertainties of the order of 30%–35% over the whole range, the parton-shower-based predictions show only a variation of below 10% at the beginning of the spectrum while the uncertainty grows up to 35% at high p_T once the real matrix elements dominate the spectrum again. Over the whole plotted range the scale uncertainties dominate over the matching related ones. However, the latter are larger for MG5_aMC@NLO as compared to the POWHEG-BOX and amount to roughly 15%.

The plot on the right-hand side of Fig. 7 illustrates the pseudorapidity of the hardest jet. Here, we observe that including parton-shower effects generates overall positive corrections of the order of 13%–20%. These corrections can be simply attributed to the fact that after the parton-shower evolution the number of events with at least one jet is higher than in the corresponding fixed-order NLO computation. To be precise, MG5_aMC@NLO predicts 11%, Sherpa 13%, and the POWHEG-BOX 15% more events with at least one hard jet. The small differences between MG5_aMC@NLO and Sherpa can be attributed to different shower dynamics, while the difference between the POWHEG-BOX and MG5_aMC@NLO is related to the parton-shower-matching scheme (as shower differences are minor between these two). Also notable is the reduction of
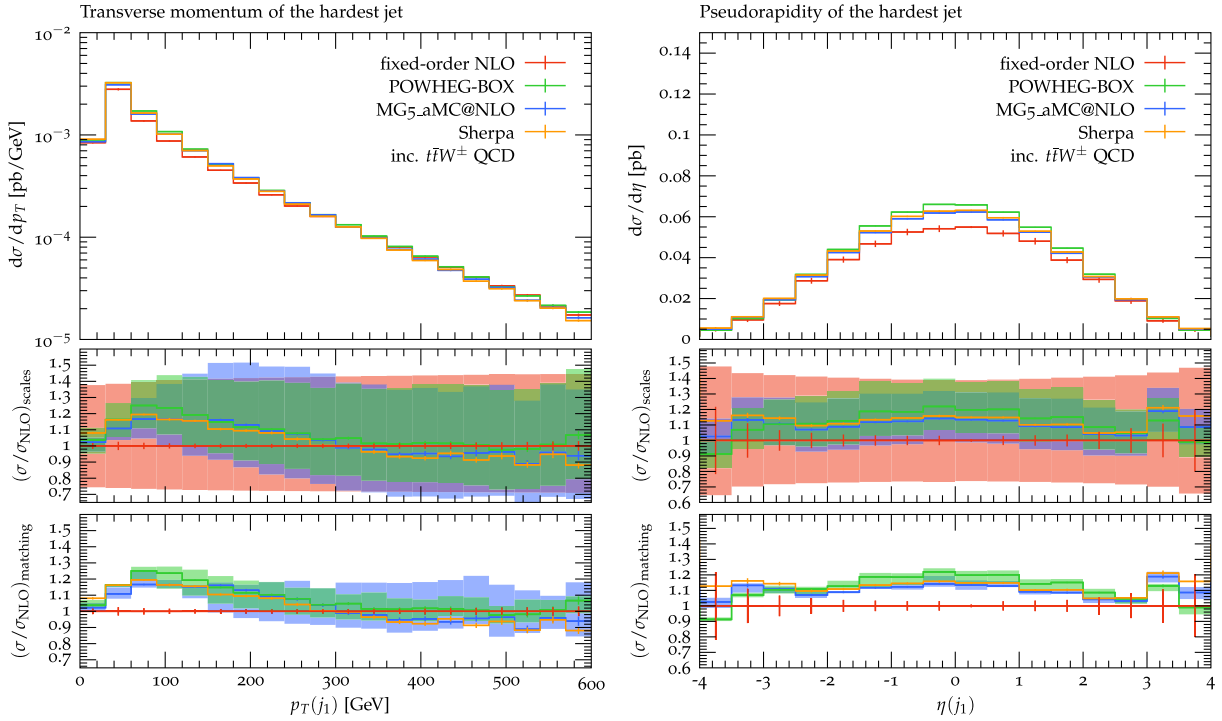
FIG. 7. Inclusive $t\bar{t}W^{\pm}$ QCD production as a function of the transverse momentum (lhs) and of the pseudorapidity (rhs) of the hardest jet for various event generators. The uncertainty bands (not shown for Sherpa) correspond to independent variations of renormalization and factorization scales (middle panel) and of the matching parameters (bottom panel).

the theoretical uncertainties by a factor of 2, from $\pm 30\%$ at fixed order to $\pm 15\%$ in the central rapidity bins once the predictions are matched to a parton shower. As we can see from the bottom panel the matching uncertainties are negligible over the whole spectrum.

2. $t\bar{t}W^{\pm}$ EW contribution

Moving on to $t\bar{t}W^{\pm}$ EW contributions to the inclusive $t\bar{t}W^{\pm}$ signature, we illustrate in the left-hand side plot of Fig. 8 the transverse momentum of the top quark $[p_T(t)]$. As this observable is already accurate to NLO we find the expected good agreement between fixed-order prediction and the POWHEG-BOX as well as MG5_aMC@NLO. On the other hand, the Sherpa prediction captures the shape of the distribution well but underestimates the normalization by 13% as can be seen from the corresponding bottom panel. The reason for the discrepancy is that the Sherpa result is based on merging of tree-level matrix elements for $t\bar{t}W^{\pm}$ and $t\bar{t}W^{\pm}j$ and therefore misses higher-order loop corrections, as well as parts of the dominant real radiative corrections below the merging scale. The estimated theoretical uncertainties from scale variations is around $\pm 20\%$–25% for fixed-order, POWHEG-BOX, and MG5_aMC@NLO result. As the distribution is NLO accurate we only observe a mild dependence on the matching scheme of at most 10%. A slightly different situation is encountered when considering the invariant mass of the

top-quark pair ($M_{t\bar{t}}$) shown on the right-hand side of Fig. 8. In this case, only the POWHEG-BOX agrees with the fixed-order result within the statistical uncertainties nearly over the whole plotted range. Results obtained with MG5_aMC@NLO show shape differences with respect to the fixed-order result. At the beginning of the spectrum MG5_aMC@NLO is 13% higher, while it is lower in the high-energy tail of the fixed-order distribution at $M_{t\bar{t}} \approx 1$ TeV by nearly 20%. As in the previous case Sherpa underestimates the normalization by about -12%. Nevertheless, within the scale uncertainties of each prediction, which amount to 16% at the beginning of the spectrum and 21% at the end of the plotted range, all distributions agree well with each other. Moreover, we find that the observable is very stable with respect to matching related parameters, as these uncertainties are almost negligible.

In Fig. 9 we further consider the transverse momentum (lhs) and the pseudorapidity (rhs) of the hardest jet. Contrary to the $t\bar{t}W^{\pm}$ QCD predictions we observe large differences between the various predictions. For the transverse momentum distribution of the leading jet we find that the POWHEG-BOX predicts a slightly softer spectrum than the fixed-order result with $+12\%$ corrections in the first bin, while for the remaining spectrum the curve is nearly a constant -5% below the fixed-order one. It is the parton-shower evolution that softens the spectrum slightly and thus these corrections are of higher order. MG5_aMC@NLO generates a much harder intermediate spectrum with
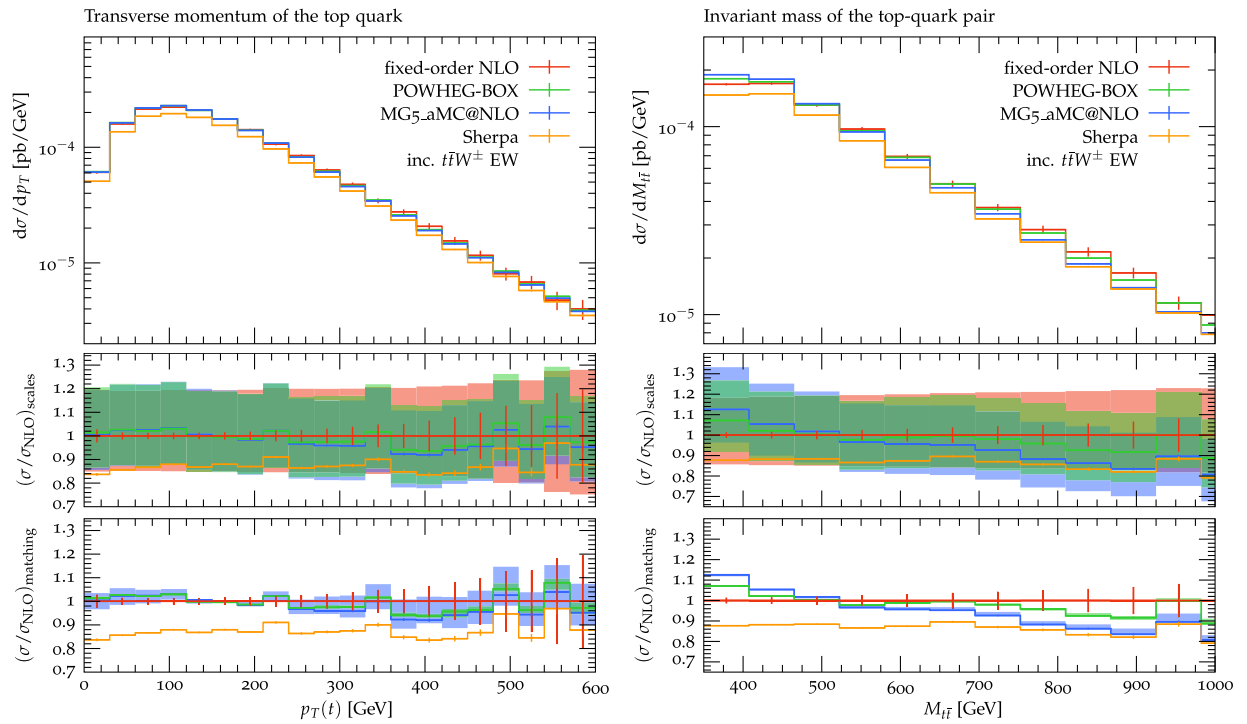
FIG. 8.   Inclusive $t\bar{t}W^{\pm}$ EW production as a function of the transverse momentum of the top quark (lhs) and the invariant mass of the top-quark pair (rhs) for various event generators. The uncertainty bands (not shown for Sherpa) correspond to independent variations of renormalization and factorization scales (middle panel) and of the matching parameters (bottom panel).
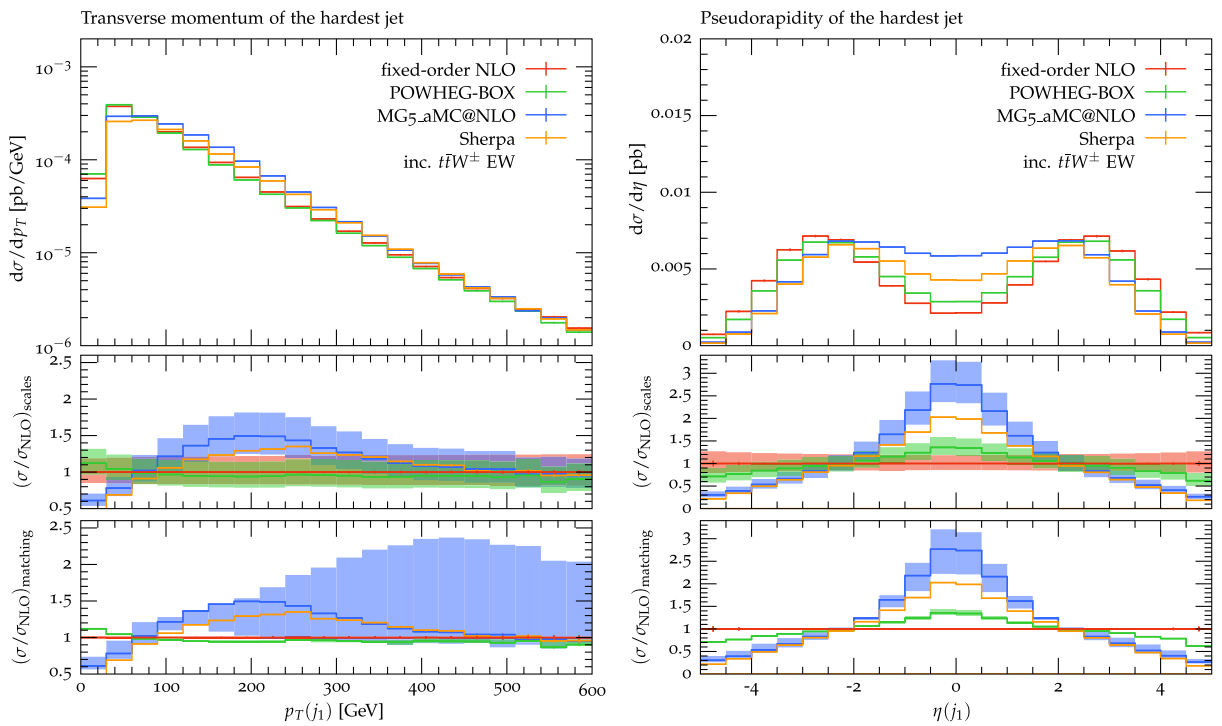

FIG. 9.   Inclusive $t\bar{t}W^{\pm}$ EW production as a function of the transverse momentum (lhs) and of the pseudorapidity (rhs) of the leading jet for various event generators. The uncertainty bands (not shown for Sherpa) correspond to independent variations of renormalization and factorization scales (middle panel) and of the matching parameters (bottom panel).

corrections up to $+50\%$ around $p_T \approx 200$ GeV and falls back to the fixed-order result toward the end of the plotted range. Last, the Sherpa prediction shows similar features to MG5_aMC@NLO but less pronounced. The theoretical uncertainties are of the order of $\pm 20\%$ for the fixed-order as well as the parton-shower-matched predictions. However, because of the severe shape differences the uncertainty band of MG5_aMC@NLO barely overlaps with the fixed-order or the POWHEG-BOX result for intermediate values of the transverse momentum. Furthermore, we see that the POWHEG-BOX results are very stable with respect to the damping parameters as variations at the level of only 5% are visible. Contrary, the MG5_aMC@NLO result depends strongly on the initial shower scale which dominates the theoretical uncertainties from $p_T \gtrsim 150$ GeV.

Finally, also in the case of the hardest-jet pseudorapidity distribution we observe quite different predictions. While the POWHEG-BOX prediction is still the closest to the fixed-order NLO result we note shape differences, with deviations of nearly $+30\%$ in the central region as well as -30% in the forward rapidity regions. The MG5_aMC@NLO prediction generates even larger corrections, which reach up to a factor of 2.8 in the central region and are suppressed by nearly -70% in the forward regions, while the Sherpa prediction lies in between MG5_aMC@NLO and the POWHEG-BOX. Indeed, Sherpa agrees with the MG5_aMC@NLO prediction in the very forward region, while it is closer to the POWHEG-BOX for the central rapidity bins. The significant shape differences also lie mostly outside of the estimated uncertainty bands. Let us remind the reader that, as illustrated in Fig. 5, the POWHEG-BOX reproduces the fixed-order distribution well when no shower evolution is taken into account. Therefore, the significant corrections in the central rapidity region can be attributed to formally higher-order corrections generated by the parton shower. This can be also deduced from the dependence of the MG5_aMC@NLO results on the initial shower scale. We observe a large shape differences of around 20% in the central rapidity bins by varying the shower scale, which is comparable to the scale uncertainties.

3. Combined $t\bar{t}W^{\pm}$ QCD + EW contribution

As we have seen the $t\bar{t}W^{\pm}$ QCD and EW contributions differ quite substantially in size, in their associated uncertainties, and in their sensitivity to the parton-shower-matching schemes, where the strongest modeling dependence has been found in the EW production channel. Thus the question arises of how much of these effects are visible in the total predictions once EW and QCD contributions are combined. To highlight the overall size of the EW contribution we list in Table I the total cross sections for the QCD and EW contributions separately as well as combined, both for the fixed-order NLO computation and for

the three generators considered in our study.[4] We observe that the inclusion of the EW contribution is an 8%–9% correction on top of the dominant QCD contribution, while the theoretical uncertainties estimated via scale variations of the QCD contribution amounts to already $\pm 11\%$. Therefore, in order to have a visible effect of the EW contribution on differential distributions one has to focus on phase space regions where the EW production mode is enhanced with respect to the QCD one. In the following we show two representative observables that illustrate the impact of the EW contribution on combined differential distributions using our POWHEG-BOX implementation. In Fig. 10 we show again the pseudorapidity of the hardest jet, for the three considered Monte Carlo generators on the left-hand side while on the right-hand side the same distribution is shown as predicted by the $t\bar{t}W^{\pm}$ QCD contribution only and the combined $t\bar{t}W^{\pm}$ QCD + EW contribution. The overall agreement between the different predictions is good with shape differences of only 10% in the very forward region. As can be deduced from the right plot of Fig. 10 the EW contribution becomes sizable in the forward region by modifying the shape of the distribution by nearly 80% and thus the observed shape differences between the various predictions are related to the modeling discrepancies in the EW contribution. Even though the theoretical uncertainties are dominated by missing higher-order corrections and amount to roughly $\pm 15\%$ the inclusion of the EW contribution represents a systematic shift of at least $+5\%$. As a second example we show in Fig. 11 the inclusive cross section as a function of the number of jets (N_{jets}), both light and b jets. For the first three bins we find excellent agreement between the three generators. Afterward the predictions diverge and the POWHEG-BOX predicts the smallest while Sherpa the largest cross section for high jet multiplicities with differences as large as 60% for the jet bin with six or more jets. However, while the first three bins are dominated by uncertainties stemming from missing higher-order corrections the remaining bins are mostly affected by parton-shower effects whose uncertainty can be large. Indeed, while in the case of POWHEG-BOX the matching uncertainty does not exceed 5%, in the MG5_aMC@NLO case the spectrum is dominated by the dependence on the initial shower scale μ_Q that can easily account for the aforementioned shape differences. Finally, we want to notice that even if the impact of the inclusive $t\bar{t}W^{\pm}$ EW contribution starts at $+9\%$ and increases with the number of jets to about a $+20\%$ correction on top of the QCD prediction for six and more jets, in this region the uncertainty of the QCD contribution overshadows this correction.

To summarize our findings of this section, we can say that $t\bar{t}W^{\pm}$ QCD inclusive production is rather robust with

---

[4]We remind the reader that in our setup Sherpa employs tree-level merging of matrix elements for the EW contribution and thus does not have to agree with the other generators.
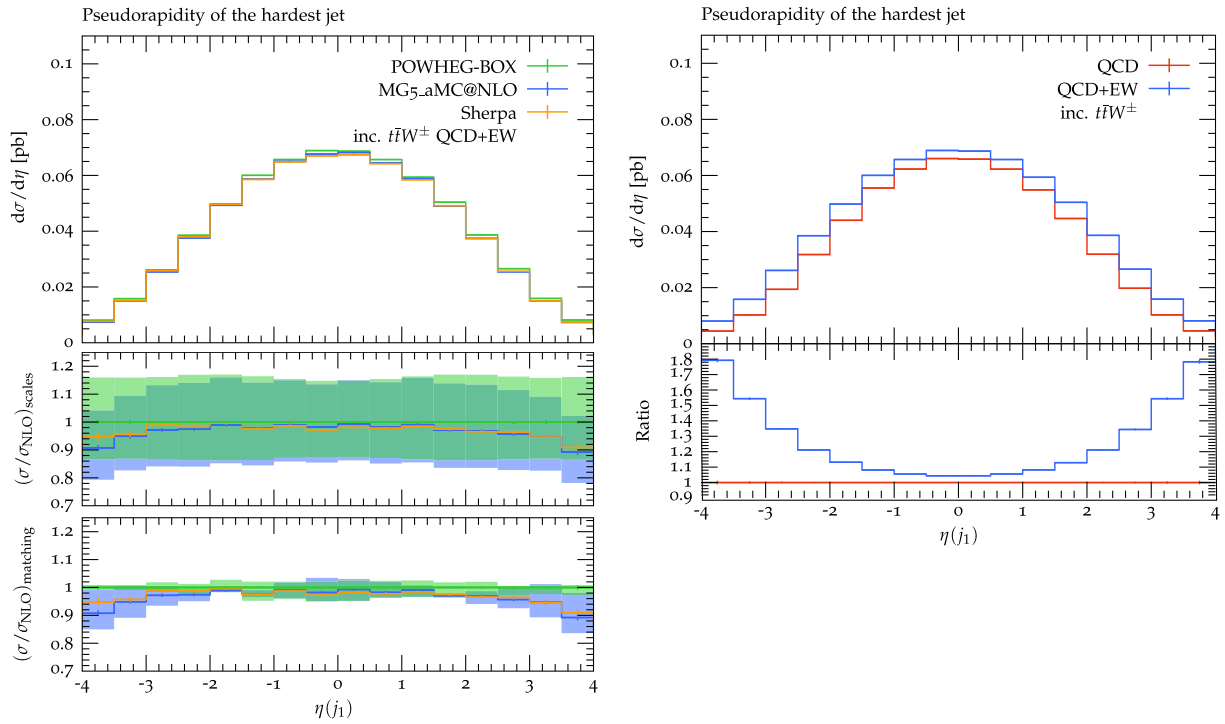
FIG. 10.   Inclusive $t\bar{t}W^{\pm}$ EW + QCD production as a function of the pseudorapidity of the leading jet shown for various event generators (lhs) and split into QCD and QCD + EW contribution (rhs). The uncertainty bands in the lhs plot (not shown for Sherpa) correspond to independent variations of renormalization and factorization scales (middle panel) and of the matching parameters (bottom panel).
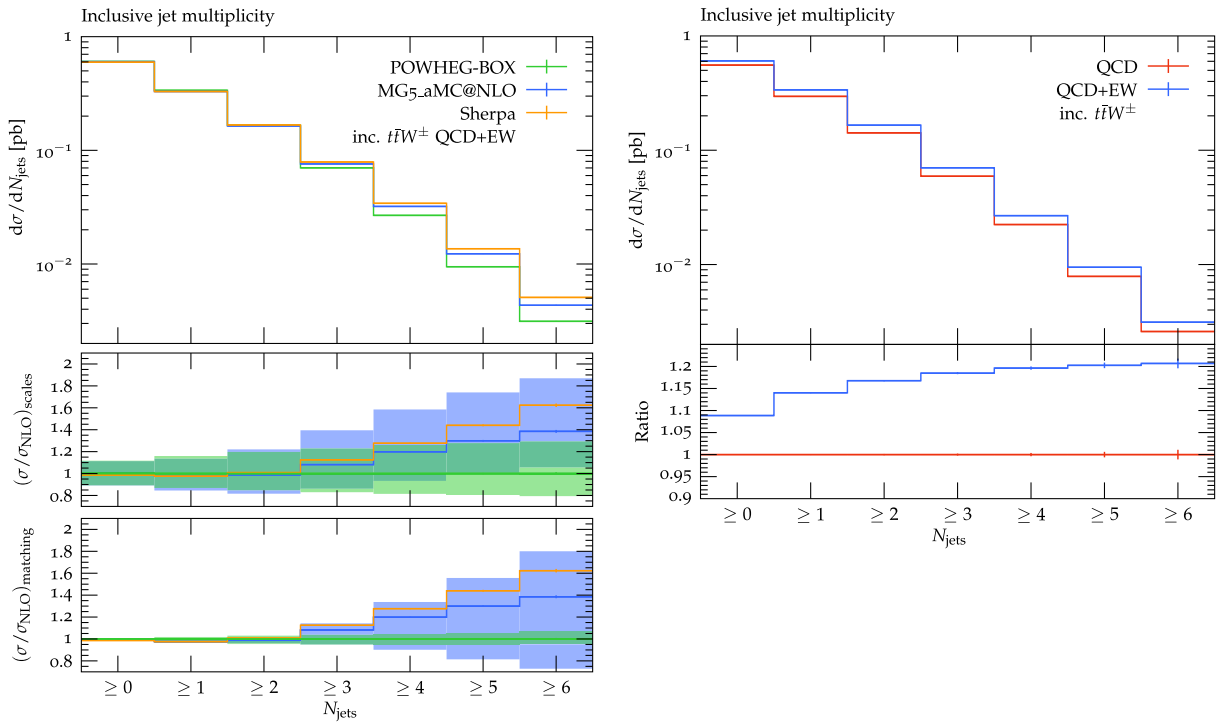

FIG. 11.   Inclusive $t\bar{t}W^{\pm}$ EW + QCD cross section as a function of the number of jets shown for various event generators (lhs) and split into QCD and QCD + EW contribution (rhs). The uncertainty bands in the lhs plot (not shown for Sherpa) correspond to independent variations of renormalization and factorization scales (middle panel) and of the matching parameters (bottom panel).

TABLE I. Inclusive $t\bar{t}W^{\pm}$ cross section contributions at NLO accuracy for fixed-order and parton-shower-matched results including the theoretical uncertainty estimated from independent scale variations. In parentheses we include the statistical error.

σ [fb]	QCD	EW	QCD + EW	$\frac{\text{QCD+EW}}{\text{QCD}}$
σ^{NLO}	$554.8(3)^{+61.5(11\%)}_{-57.4(10\%)}$	$49.0(2)^{+9.5(19\%)}_{-7.3(15\%)}$	$603.8(3)^{+71.0(12\%)}_{-65.2(11\%)}$	1.09
$\sigma^{\text{NLO+PS}}_{\text{PWG}}$	$555.6(4)^{+61.5(11\%)}_{-57.8(10\%)}$	$49.2(1)^{+9.5(19\%)}_{-7.4(15\%)}$	$604.8(4)^{+71.0(12\%)}_{-65.2(11\%)}$	1.09
$\sigma^{\text{NLO+PS}}_{\text{MG5}}$	$554.0(6)^{+60.8(11\%)}_{-57.5(10\%)}$	$49.1(1)^{+9.5(19\%)}_{-7.4(15\%)}$	$603.1(6)^{+70.4(12\%)}_{-64.8(11\%)}$	1.09
$\sigma^{\text{NLO+PS}}_{\text{Sherpa}}$	553.7(8)	42.7(1)	596.4(8)	1.08

respect to matching uncertainties and different parton-shower algorithms. On the other hand, the $t\bar{t}W^{\pm}$ EW contribution is very sensitive to different matching procedures as sizable higher-order corrections can be generated by the parton shower even for inclusive observables. This, however, might not be surprising altogether in this particular case, since the NLO corrections in $t\bar{t}W^{\pm}$ EW production are highly dominated by real radiation matrix elements and therefore the description of this process is essentially only at LO accuracy. This can also be seen from the fact that the Sherpa prediction, which in the EW case is based only on tree-level matrix elements, still recovers the main features of many observables. In addition, the EW production channel is mediated by t-channel exchanges of color singlets and could be thus also sensitive to radiation patterns of parton-shower implementations [74]. At last, we have to note that even though we observe large differences in the modeling of the $t\bar{t}W^{\pm}$ EW contribution these differences are much less visible once the QCD and EW contributions are combined.

C. Two same-sign leptons signature

In this section we focus on the experimental signature of two same-sign leptons in association with additional jets, usually denoted as $2\ell SS$. The final state is selected by requiring exactly two same-sign leptons[5] with $p_T(\ell) > 15$ GeV and $|\eta(\ell)| < 2.5$. Jets are formed using the anti-k_T jet algorithm with a separation parameter of $R = 0.4$. We further require that jets (light as well as b jets) fulfill $p_T(j) > 25$ GeV and $|\eta(j)| < 2.5$. Finally, we require at least two light jets as well as two tagged b jets.

Results shown in this section correspond to the sum of $t\bar{t}W^{\pm}$ QCD and $t\bar{t}W^{\pm}$ EW production modes which contribute to the $2\ell SS$ signature defined above. Emphasis will be placed on identifying the major sources of theoretical uncertainty from scale variation and parton-shower matching following the procedure discussed in Sec. IV A.

---

[5]We exclude τ leptons here, since these typically form different signatures at hadron collider detectors. Thus we focus on $e^{\pm}e^{\pm}$, $e^{\pm}\mu^{\pm}$, and $\mu^{\pm}\mu^{\pm}$.

For the range of parameters described in Sec. IV A and the selection cuts above, we obtain fully consistent fiducial cross sections in all the frameworks considered in our study, namely

$$\sigma^{\text{NLO+PS}}_{\text{PWG}} = 6.79(1)^{+0.84(12\%)}_{-0.75(11\%)} \,[\text{scales}]^{+0.05(1\%)}_{-0.09(1\%)} \,[\text{matching}] \text{ fb},$$

$$\sigma^{\text{NLO+PS}}_{\text{MG5}} = 6.80(1)^{+0.86(13\%)}_{-0.76(12\%)} \,[\text{scales}]^{+0.07(1\%)}_{-0.05(1\%)} \,[\text{matching}] \text{ fb},$$

$$\sigma^{\text{NLO+PS}}_{\text{Sherpa}} = 6.80(1) \text{ fb}, \tag{28}$$

where the residual uncertainty as estimated from the variation of renormalization and factorization scales (here and in the plots labeled as "*scales*") are of the order of 12%, while the impact of varying matching related parameters, i.e., the damping factors in the case of the POWHEG-BOX and the initial shower scale in the case of MG5_aMC@NLO (here and in the plots labeled as "*matching*"), is a 1% effect in both cases. The central result of Sherpa agrees perfectly with the other generators. Notice that the scale uncertainties of the fiducial cross sections in Eq. (28) amount to $\pm 12\%$ and are consistent with the corresponding ones of the total inclusive cross sections shown in Table I. This emphasizes the fact that even though the fiducial cross section is tremendously reduced by branching ratios and phase space cuts on the decay products the signature is still inclusive with respect to the production of the heavy $t\bar{t}W^{\pm}$ final state.

1. Hadronic observables

Theoretical uncertainties on the total cross sections are of course not representative of the actual uncertainties affecting differential distributions in different regions of the corresponding kinematic observables. With this in mind we will discuss in the following several distributions of phenomenological interest and emphasize how from the analysis of the residual scale and matching uncertainties we can derive indications of how to improve the corresponding theoretical predictions. All plots presented in Figs. 12–17 consist of three panels where the upper panel shows the central predictions for the three considered generators, the middle one illustrates the scale uncertainty band based on the variation of μ_R and μ_F, and the bottom one is the matching uncertainty band obtained from the variation of

damping factors and the initial shower scale μ_Q. Both scales and matching uncertainties are normalized to the central POWHEG-BOX prediction.

We start by considering the fiducial cross section as a function of the number of light ($N_{\text{l-jets}}$) or bottom ($N_{\text{b-jets}}$) jets, as shown in Fig. 12. In the case of light jets, shown on the left side of Fig. 12, we observe that MG5_aMC@NLO and Sherpa predictions align really well in all jet bins. Comparing to the POWHEG-BOX we note that predictions for at least two, three, and four light jets agree well among all generators, while starting from at least five light jets onward the POWHEG-BOX generates a softer spectrum and the deviation grows from 10% up to 47% for events with at least eight light jets, although the shape differences are within the estimated theoretical uncertainties. Scale uncertainties are slightly asymmetric and start, after symmetrization, at 12% for at least two jets and increase to 25% for the POWHEG-BOX and 29% for MG5_aMC@NLO. On the other hand, the matching uncertainties are rather different between the predictions. Varying the damping parameters in the POWHEG-BOX only leads to modifications of the cross sections of at most ±5% in the last jet bin, while variations of the initial shower scale in MG5_aMC@NLO lead to variations of up to ±47%. Thus, in the case of MG5_aMC@NLO the initial shower scale uncertainties become the dominant starting from at least six light jets.

Similar conclusions can be drawn for the distribution in the number of b jets. Beyond the first bin all three generators give slightly different predictions, where the POWHEG-BOX shows the softest spectrum and MG5_aMC@NLO the hardest, with nearly 50% deviations with respect to the POWHEG-BOX distribution for events with five b jets. However, Monte Carlo errors become sizable in this region as well. Sherpa resembles more closely the POWHEG-BOX spectrum over the whole range with differences of at most 25%. As for the case of light jets, the large deviations between the generators are compatible with the estimated theoretical uncertainties. While scale variations in the first bin still amount to 12% uncertainties they increase rapidly to 19%–24% for each prediction. Also matching uncertainties increase tremendously for more than three b jets and show that these regions are clearly dominated by the parton shower, as expected for this particular observable. In general, also for other less obvious observables, a sudden strong dependence on the initial shower conditions indicate that these regions are dominated by the parton shower instead of the underlying NLO computation.

Turning to other exclusive observables we compare the modeling of fiducial differential distributions for the considered event generators starting with the invariant mass spectrum of the two hardest jets $M_{j_1 j_2}$ depicted on the left of Fig. 13. It is remarkable to see the pronounced
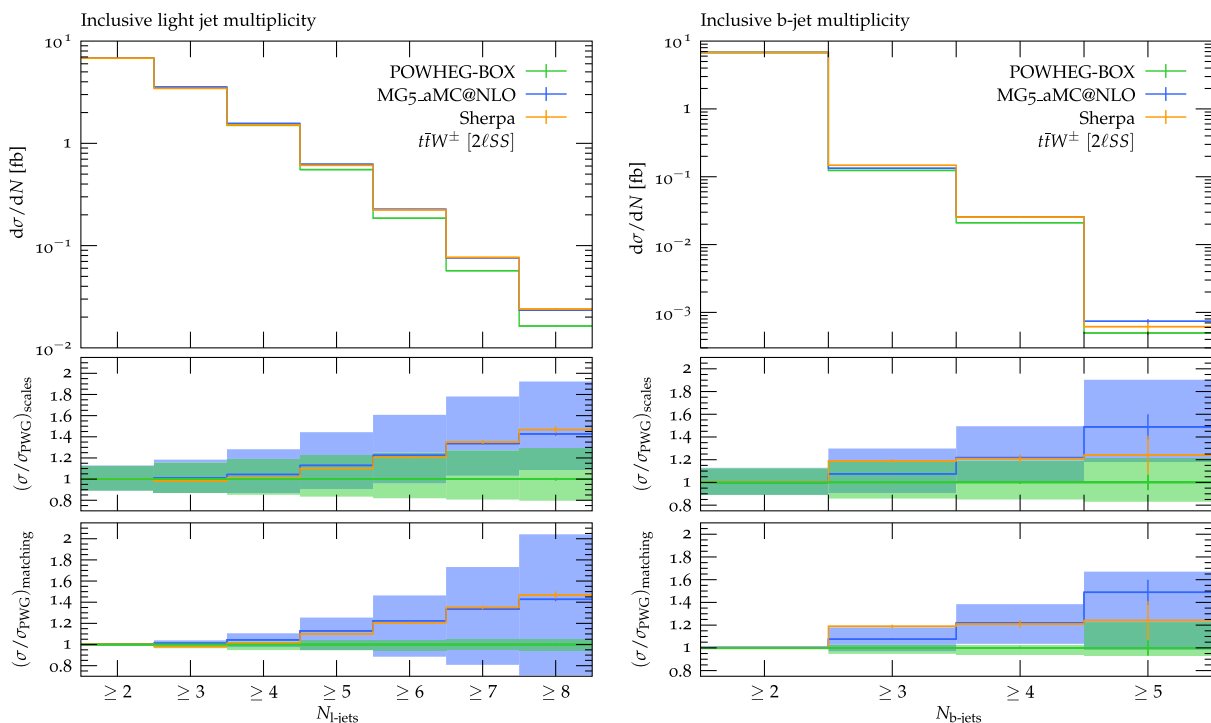

FIG. 12. Inclusive cross section in the $2\ell SS$ fiducial region as a function of the number of light jets (lhs) and the number of b jets (rhs) for various event generators. The uncertainty bands (not shown for Sherpa) correspond to independent variations of renormalization and factorization scales (middle panel) and of the matching parameters (bottom panel).
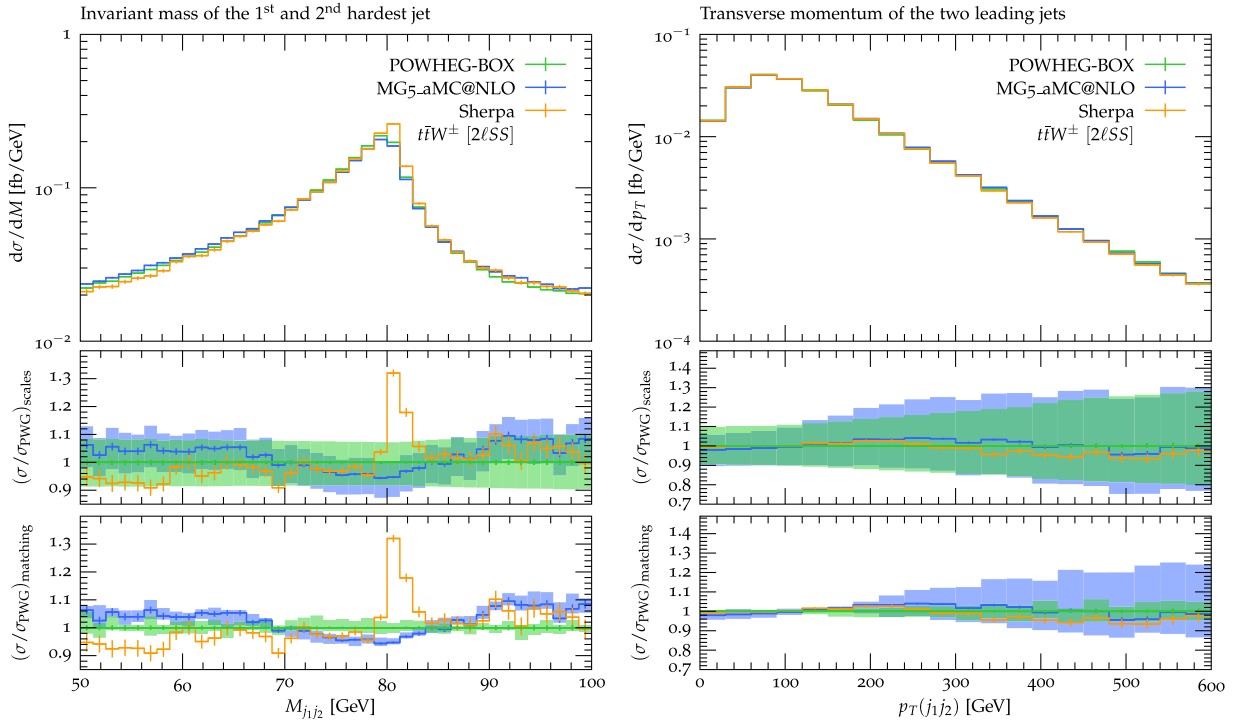
FIG. 13. Differential cross section in the $2\ell SS$ fiducial region as a function of the invariant mass (lhs) and the transverse momentum (rhs) of the two leading light jets. The uncertainty bands (not shown for Sherpa) correspond to independent variations of renormalization and factorization scales (middle panel) and of the matching parameters (bottom panel).

Breit-Wigner shape of the W boson, which suggests how the hardest jets in an event are predominantly generated by the hadronic decay of one of the W bosons. More information can be derived from a closer inspection of the p_T distribution of these jets, as we will discuss in the following. With respect to the POWHEG-BOX curve, the MG5_aMC@NLO prediction for the $M_{j_1j_2}$ distribution shows a slightly different shape with deviations of the order of 5%. MG5_aMC@NLO is slightly more off shell as can be seen by the depletion of events in the resonance region by about 5%. Sherpa on the other hand is considerable more on shell with 32% more events on the W resonance. The scale uncertainties are nearly constant for MG5_aMC@NLO and of the order of 7% in the plotted range. For the POWHEG-BOX prediction scale uncertainties are constant and of the order of 8% below $M_{j_1j_2} \approx M_W$ and increase mildly to 10% at the end of the spectrum. The matching uncertainties are for the MC@NLO or POWHEG scheme both at most 4%. The small impact of the shower scale variation can be understood from the fact that PYTHIA8 preserves the momentum of resonant decaying particles. Therefore, the available phase space for further radiation is naturally limited by a shower scale $\mu_Q \lesssim M_W$, which is considerable smaller than $\mu_Q = H_T/2$ and thus the radiation pattern of a hadronic decaying W can to a large extent be independent of the variation of the initial shower scale we have chosen.

On the right-hand side of Fig. 13 we also show the overall transverse momentum distribution of the two hardest light jets $p_T(j_1j_2)$. All three predictions agree remarkably well over the whole plotted range with only minor shape differences, with deviations of up to 5%. The dominant contribution to the theoretical uncertainties originates from missing higher-order corrections. They amount to at least $\pm 10\%$ and increase with growing transverse momentum to -27% and $+30\%$ at $p_T \approx 600$ GeV. Below $p_T \lesssim 180$ GeV the matching uncertainties are about 2%–3% for both the MC@NLO and POWHEG schemes. Above, the initial shower scale dependence grows steadily to 20%, while the dependence of damping factors in the POWHEG-BOX stays below 5%. The increase in the theoretical uncertainties with p_T and in particular above $p_T \geq 180$ GeV suggests that the spectrum is sensitive to the real radiation and thus one of the leading jets actually originates from an emission in the production of the $t\bar{t}W^{\pm}$ final state. Below a transverse momentum value of 180 GeV the spectrum is dominated by radiative top-quark decays. This explains the reduced scale dependence of the POWHEG-BOX and MG5_aMC@NLO predictions in this region, since this part of the distribution is inclusive with respect to the production of the $t\bar{t}W^{\pm}$ system. Radiative top decays also account for the insensitivity on the initial shower scale of the predictions because PYTHIA8 preserves the top-quark resonance and thus a natural shower scale of

$\mu_Q \approx m_t \ll H_T/2$ is in place. To investigate the modeling of the first and second hardest light jets in more detail, we show in Fig. 14 the distributions in their individual transverse momentum [$p_T(j_1)$ and $p_T(j_2)$, respectively]. For both observables the shapes of the different generator's predictions agree well with each other. In the case of the hardest light jet, differences do not exceed 10%, while for the transverse momentum of the second hardest light jet deviations at the level of 10% are visible and can become as large as 20% in the tail of the distribution for MG5_aMC@NLO. The two transverse momentum spectra however exhibit rather different theoretical uncertainties. For the hardest light jet the uncertainties are dominated by scale uncertainties that start around 6%–8% and increase up to 26%–29% in the tail of the distribution. Note that the POWHEG-BOX scale uncertainties start slightly larger but grows lower than those of MG5_aMC@NLO. On the other hand, the matching uncertainties for the POWHEG-BOX are below ±5% variation over the whole spectrum, while for MG5_aMC@NLO the uncertainties are of comparable size only below $p_T \approx 180$ GeV but grow to about +27% and −9% for higher p_T. The still modest impact of the shower scale can be attributed to the fact that the tail of the spectrum is stabilized by the NLO real radiation and thus depends less on the shower evolution. The scale dependence for the transverse momentum distribution of the second hardest light jet behaves identically to the previous case. At the beginning there are uncertainties of the order of

7%–9% that rise to 30%–33% in the tail. However, the matching uncertainties dominate quickly the theoretical uncertainty of the MG5_aMC@NLO prediction, while, as in the previous cases, the POWHEG-BOX predictions show damping uncertainties below 5% over the full p_T range. While the MG5_aMC@NLO uncertainties are compatible with the POWHEG-BOX only up to 120 GeV the corresponding shower scale dependence increases dramatically and generates corrections between −23% and +91%. Clearly, all shape differences of the three different generators are within that uncertainty.

After discussing light-jet distributions we turn now to b jets that are predominantly generated in the decay of top quarks and are thus a good testing ground to compare different top-quark modeling strategies. Starting with the transverse momentum of the hardest b jet $p_T(b_1)$ shown on the left-hand side of Fig. 15, we observe small shape differences between the various predictions especially in the beginning of the distribution. The POWHEG-BOX prediction is slightly harder than MG5_aMC@NLO and Sherpa; however, the shape difference is well below 10% and the prediction of the b jet spectrum is sensitive to the modeling of top-quark decays [75] as well as to the modeling of radiation from b quarks in the parton shower. However, the dominant source of uncertainty remains the missing higher-order corrections which amount to 10%–18%, as shown by the scale dependence of the high-p_T spectrum. Regarding the matching uncertainties one can
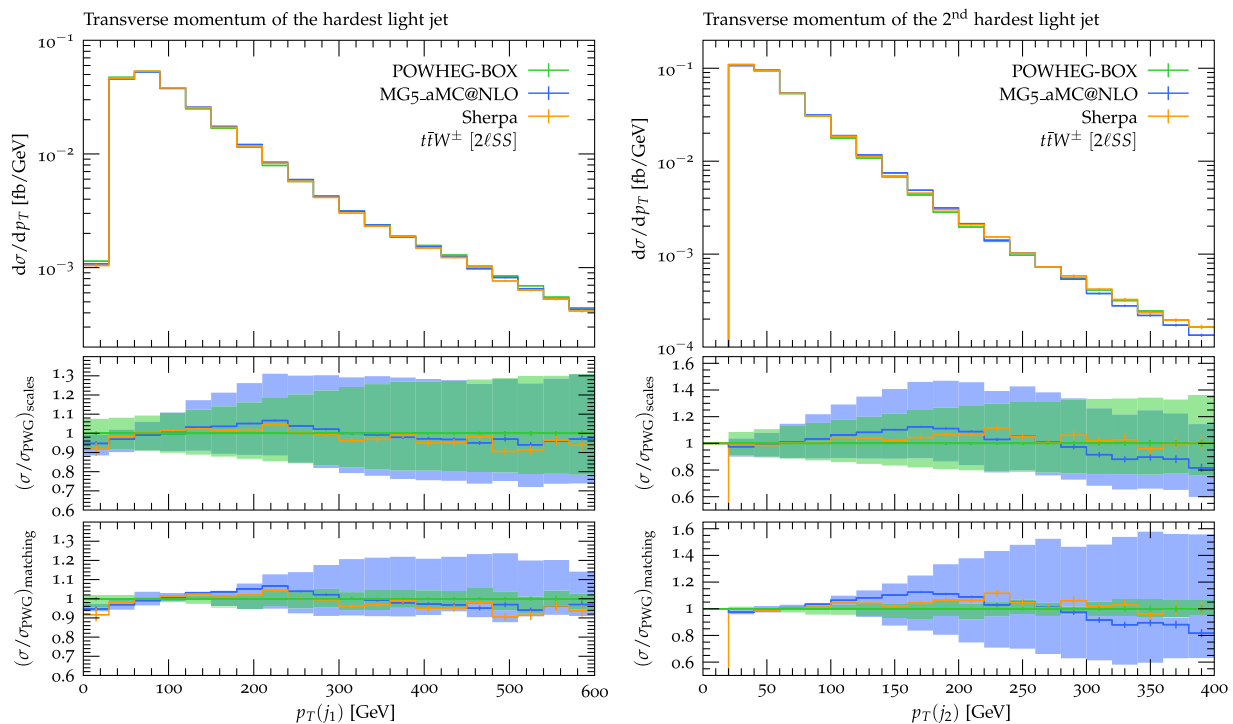

FIG. 14.   Differential cross section for the $2\ell SS$ fiducial region as a function of the transverse momentum of the hardest (lhs) and second hardest (rhs) light jet. The uncertainty bands (not shown for Sherpa) correspond to independent variations of renormalization and factorization scales (middle panel) and of the matching parameters (bottom panel).
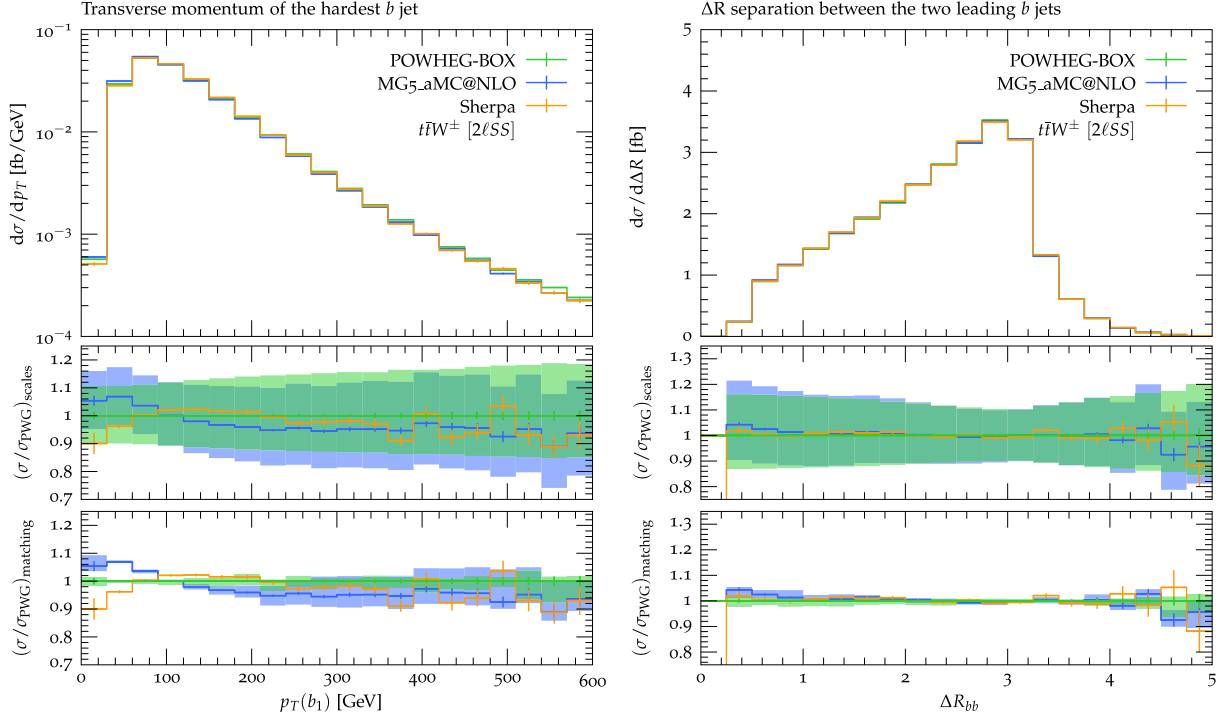
FIG. 15.   Differential cross section for the $2\ell SS$ fiducial region as a function of the transverse momentum of the hardest b jet (lhs) and the ΔR separation between the two leading b jets (rhs). The uncertainty bands (not shown for Sherpa) correspond to independent variations of renormalization and factorization scales (middle panel) and of the matching parameters (bottom panel).

note that the POWHEG-BOX predictions show in general a very reduced dependence on the damping parameters, while MG5_aMC@NLO obtains uncertainties as large as 8% in the tail of the distribution.

Additionally, on the right-hand side of Fig. 15 we show the ΔR_{bb} separation of the two hardest b jets. As can be seen from the shoulder in the distribution, the two leading b jets tend to be generated most of the time in a back-to-back configuration, which is typical for top-quark decays, whereas jets originating from a collinear $g \to b\bar{b}$ splitting in the parton shower would peak for small values of ΔR_{bb}. The predictions of all three generators are identical, and uncertainties are largely compatible and dominated by scale sensitivity. Scale uncertainties are the smallest around the peak at $\Delta R_{bb} \approx 3$ where they amount to $\pm 10\%$, while toward the beginning and the end of the spectrum they increase to about 18%. Matching uncertainties are for the POWHEG-BOX as well as MG5_aMC@NLO below 5% over the whole spectrum.

2. Leptonic observables

We now focus on leptonic observables, such as the transverse momentum $p_T(\ell\ell)$ and the invariant mass $M_{\ell\ell}$ spectrum of the two same-sign lepton pair that are shown in Fig. 16. These observables are only indirectly affected by QCD corrections, because the leptons will only recoil against further emissions in the parton-shower evolution. Nonetheless, these observables are crucial to illustrate the

dynamical correlations between the decay of the prompt W boson and of the top quark and, therefore, might be sensitive to the overall shower evolution. For the transverse momentum distribution shown on the left of Fig. 16 we observe that Sherpa and POWHEG-BOX predictions are essentially identical within the Monte Carlo uncertainty. In contrast, MG5_aMC@NLO shows a clear but very small shape difference with respect to the POWHEG-BOX. The distribution is clearly affected mostly by scale variations at a level of 10% over the whole range. Matching uncertainties, on the other hand, are negligible at the beginning and increase steadily toward the end of the spectrum where they become comparable in size with the scale uncertainties. For the case of the invariant mass spectrum of the lepton pair, depicted on the right of Fig. 16, we find again very good agreement between all generators over the whole range. The theoretical uncertainties are larger as compared to the transverse momentum distribution. Here, scale uncertainties start at 10% and increase up to 25% at the end of the spectrum. In addition, the spectrum is not very sensitive to the parton-shower evolution as the corresponding uncertainties are below 5% for both MG5_aMC@NLO and the POWHEG-BOX.

Additionally, we show in Fig. 17 the azimuthal angle between the two same-sign leptons $\Delta\phi_{\ell\ell}$ which is sensitive to spin correlations. Let us note at this point that the observed spin correlations in our case have a different origin than those typically studied in top-quark pair
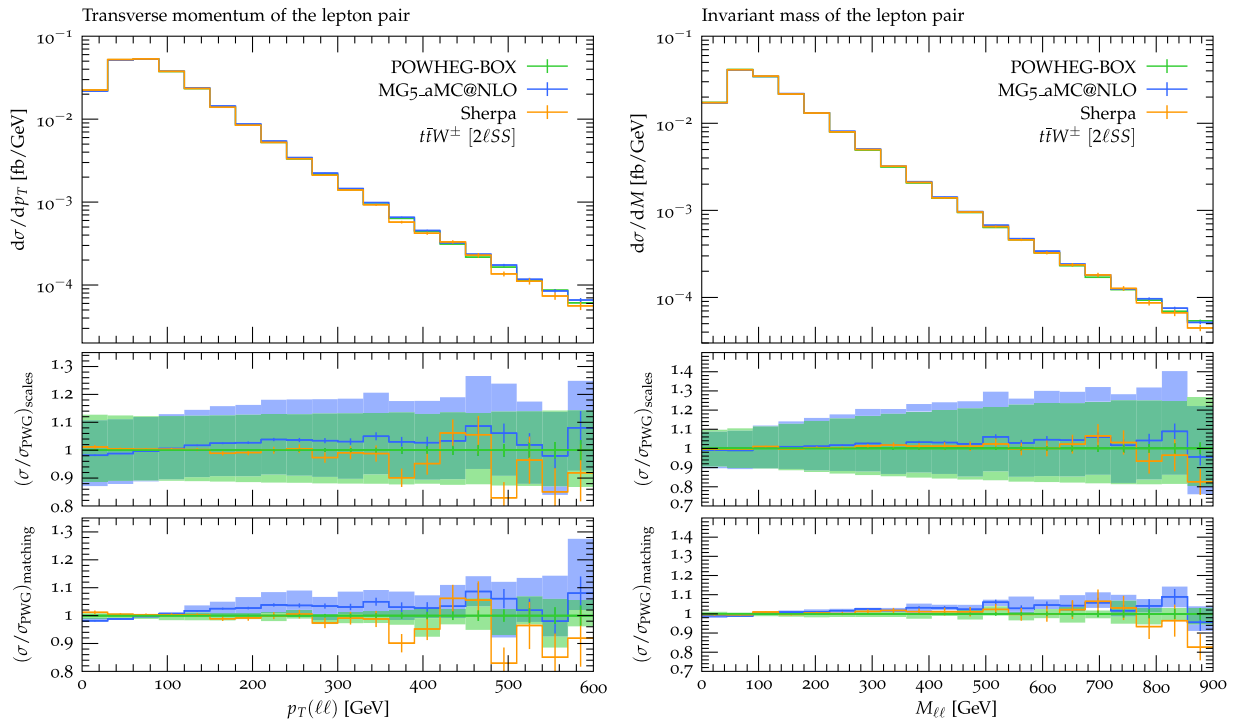
FIG. 16.   Differential cross section for the $2\ell SS$ fiducial region as a function of the transverse momentum (lhs) and the invariant mass (rhs) of the same-sign lepton pair. The uncertainty bands (not shown for Sherpa) correspond to independent variations of renormalization and factorization scales (middle panel) and of the matching parameters (bottom panel).
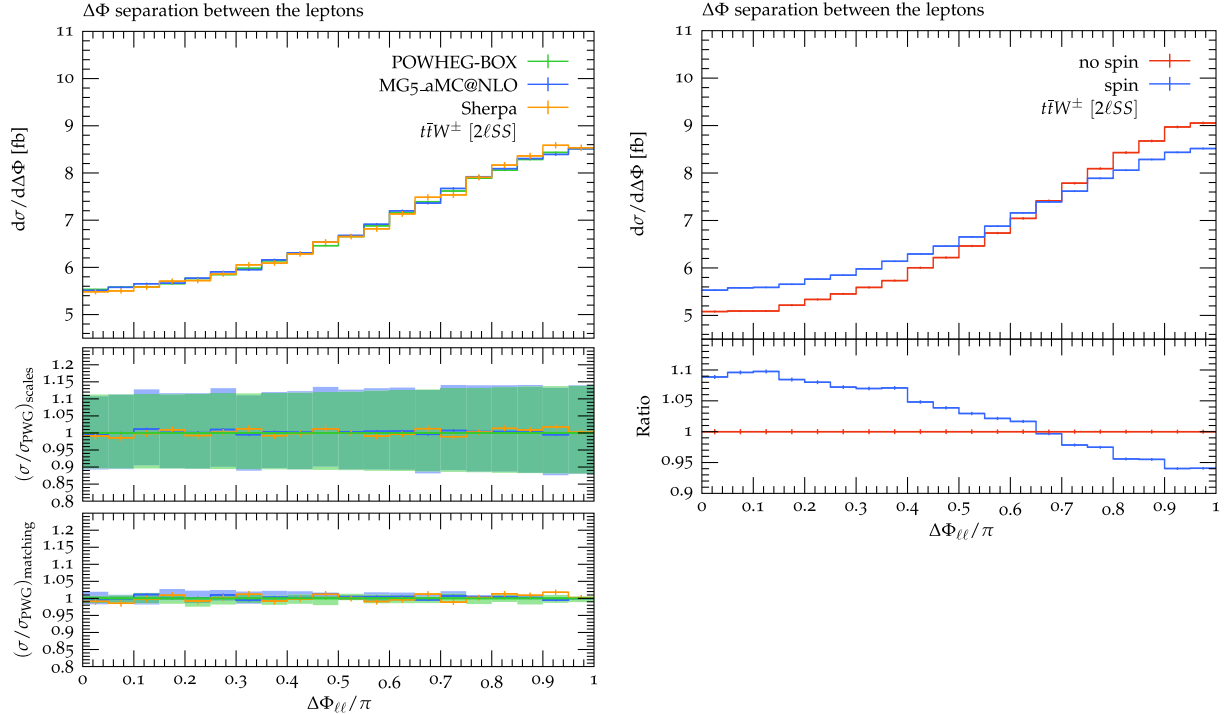

FIG. 17.   Differential cross section for the $2\ell SS$ fiducial region as a function of the azimuthal angle $\Delta\Phi_{ll}$ between the two same-sign leptons (lhs) and the impact of spin correlations in the decay modeling (rhs). The uncertainty bands in the lhs plot (not shown for Sherpa) correspond to independent variations of renormalization and factorization scales (middle panel) and of the matching parameters (bottom panel).

production [76–81]. In top-pair production the dilepton pair originating from the top-quark decays are spin correlated. In our case however, since we are considering signatures with same-sign leptons, only one lepton emerges from a top-quark decay, while the other one is produced by the decay of the prompt W boson. At the same time, it is exactly the presence of the prompt W boson that fully polarizes the top quarks [1], and as a consequence $\Delta\Phi_{\ell\ell}$ depends on the spin correlation between them. To highlight the importance of spin correlations, in the right-hand side plot of Fig. 17 we show POWHEG-BOX predictions that either include or neglect spin correlations in the decay modeling for the $2\ell SS$ final state. We observe that spin correlations lead to a shift in the spectrum, where events are shifted from the upper end of the spectrum at $\Delta\Phi_{\ell\ell} \approx \pi$ to the opposite end. The induced corrections to the distribution can reach up to 10% for $\Delta\Phi_{\ell\ell}/\pi \lesssim 0.15$. Similar effects are found in other leptonic observables (either dimensionless or dimensionful).

3. Impact of $t\bar{t}W^{\pm}$ EW contributions

We conclude this section by analyzing the impact of the EW production mode of the $t\bar{t}W^{\pm}$ final state on the $2\ell SS$ signature under consideration using our POWHEG-BOX implementation. In this context, we would like to stress that, while we highlight in the following the few special cases where the $t\bar{t}W^{\pm}$ EW contribution becomes significant and cause visible shape modifications, for most observables the inclusion of the $t\bar{t}W^{\pm}$ EW process amounts to a rather flat +10% correction at the differential level. Since the EW production mode enhances the production of light jets in the forward region, as can be seen from the pseudorapidity

distribution in Fig. 10, we expect the most severe impact in light-jet observables.

To illustrate this point, we show in the left-hand side plot of Fig. 18 the invariant mass distribution of the leading two light jets $M_{j_1 j_2}$ as predicted by the $t\bar{t}W^{\pm}$ QCD contribution only and the total $t\bar{t}W^{\pm}$ QCD + EW contribution. The bottom panel shows the ratio with respect to only the $t\bar{t}W^{\pm}$ QCD contribution. Below $M_{j_1 j_2} \lesssim 100$ GeV we see that the $t\bar{t}W^{\pm}$ EW contribution is small, about a +8% correction, which can be understood from the fact that this region should be dominated by jets originating from the hadronically decaying W boson instead of jets emitted in the production process. However, above 100 GeV the $t\bar{t}W^{\pm}$ EW contribution starts to grow until it reaches a quite significant +25% correction at the end of the plotted range. Also in the $\Delta R_{j_1 j_2}$ separation between the leading light jets, shown on the right-hand side of Fig. 18, we can see a strong impact of the $t\bar{t}W^{\pm}$ EW contribution. Below $\Delta R_{j_1 j_2} \approx \pi$ the additional contribution is small between 8% and 12% and starts growing rapidly beyond that point. In fact, the $t\bar{t}W^{\pm}$ EW contribution generates corrections of the order of 50% at $\Delta R_{j_1 j_2} \approx 5$ which highlights the fact that this contribution preferably populates the forward regions.

To further highlight the impact of the EW contribution we study jets in the forward region. To this end we look for events that have passed the selection cuts specified in Sec. IVA and have additional jets in the forward region defined by

$$p_T(j) > 25 \text{ GeV}, \qquad 2.5 \leq |\eta(j)| \leq 5.0, \qquad (29)$$

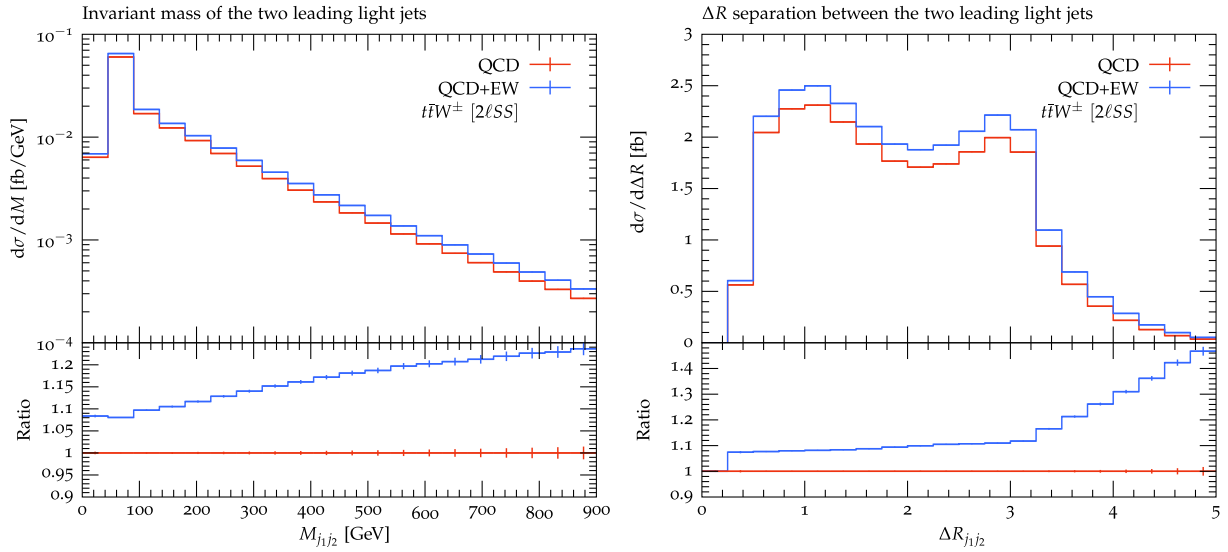where we do not distinguish between light or b jets.

FIG. 18. Differential cross section for the $2\ell SS$ fiducial region as a function of the invariant mass (lhs) and ΔR separation between the two hardest lights jets (rhs). The predictions based only on $t\bar{t}W^{\pm}$ QCD production are given in red while the total $t\bar{t}W^{\pm}$ QCD + EW contributions are shown in blue. The bottom panel shows the percentage change in the shape of the distribution.
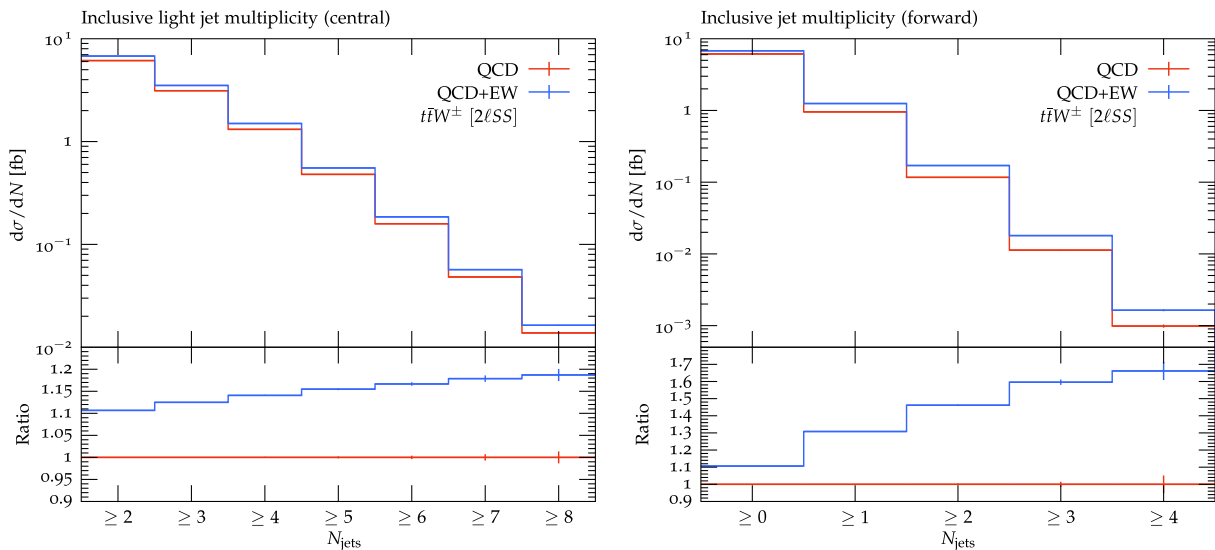
FIG. 19. The inclusive cross section for the $2\ell SS$ fiducial region as a function of the number of hard jets in the central phase space volume (lhs) and in the forward region (rhs). The predictions based only on $t\bar{t}W^{\pm}$ QCD production are given in red while the total $t\bar{t}W^{\pm}$ QCD + EW contributions are shown in blue. The bottom panel shows the percentage change in the shape of the distribution.

In Fig. 19 we show the inclusive cross section as a function of the number of jets in the forward region (rhs) and contrast it with the corresponding plot in the central region (lhs). In the central phase space volume the $t\bar{t}W^{\pm}$ EW contribution only has a very mild impact, and, for events with at least two light jets, this contribution amounts to 11%, while for events with at least eight light jets it grows to 19%. On the contrary, if we look at the inclusive jet multiplicities in the forward region as shown on the right plot in Fig. 19, then we see that for the first bin an 11% correction is visible that then quickly increases up

to 66% for events that have at least four additional forward jets.

Last we study the impact on the transverse momentum spectrum of the leading light jet, $p_T(j_1)$, in the central and forward regions as depicted in Fig. 20. As before, in the central phase space volume we find a rather constant correction of 9%–11% over the whole range of the plotted spectrum. The maximal corrections of 11% are obtained around $p_T \approx 200$ GeV. On the other hand, the hardest forward jet receives large corrections from $t\bar{t}W^{\pm}$ EW production. Essentially starting from 17% corrections at
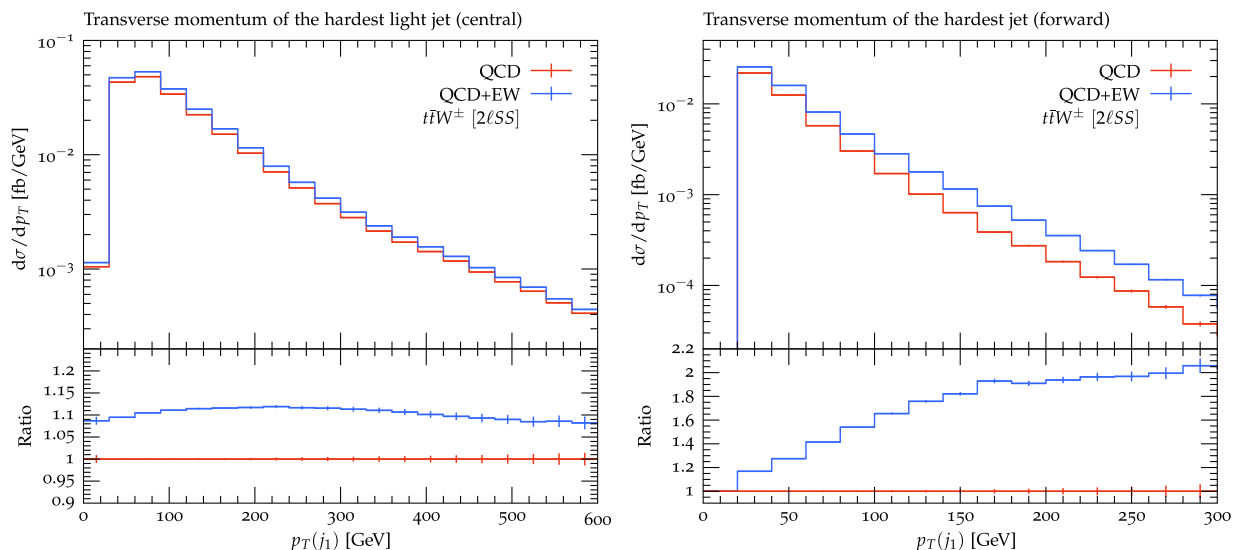

FIG. 20. Differential cross section for the $2\ell SS$ fiducial region as a function of the transverse momentum of the leading jet in central phase space volume (lhs) and in the forward region (rhs). The predictions based only on $t\bar{t}W^{\pm}$ QCD production are given in red while the total $t\bar{t}W^{\pm}$ QCD + EW contributions are shown in blue. The bottom panel shows the percentage change in the shape of the distribution.

the beginning of the distribution the $t\bar{t}W^{\pm}$ EW contribution gives rise to 100% corrections for $p_T \gtrsim 200$ GeV.

V. CONCLUSIONS

In this paper we have presented a new NLO parton-shower Monte Carlo event generator for the hadronic production of a top-quark pair in association with a $W^{\pm}$ boson taking into account the dominant NLO corrections at $\mathcal{O}(\alpha_s^3 \alpha)$ and $\mathcal{O}(\alpha_s \alpha^3)$. Decays of unstable particles are included at leading order retaining spin-correlation effects.

Motivated by the current tension [6] between the state-of-the-art SM predictions for the $t\bar{t}W^{\pm}$ cross section and the corresponding measurement derived when $t\bar{t}W^{\pm}$ is extracted from a combined signal and background fit in $t\bar{t}H$ analyses, we performed a detailed generator comparison involving the POWHEG-BOX, MG5_aMC@NLO, and Sherpa. A comparison at the level of on-shell $t\bar{t}W^{\pm}$ production has revealed good agreement for the $\mathcal{O}(\alpha_s^3 \alpha)$ production mode, while the $\mathcal{O}(\alpha_s \alpha^3)$ contribution is very sensitive to the details of a given generator setup. Furthermore, a comparison has been made at the fully decayed stage for a fiducial phase space volume corresponding to the $2\ell SS$ signature with two same-sign leptons and both light and b jets. We provide this as a proof of concept to estimate in a more robust way the residual theoretical uncertainty on the $pp \to t\bar{t}W^{\pm}$ cross section from both fixed-order and parton-shower components, at the inclusive and fiducial level. We found good agreement between all three generators at the differential level. Theoretical uncertainties have been addressed via means of independent variations of the renormalization and factorization scales as well as matching related parameters specific of each generator, such as damping factors (POWHEG-BOX) or the initial shower scale (MG5_aMC@NLO). The investigation of the latter dependence allowed us to explain peculiar shape differences between the generators. In addition, we also investigated the impact of LO accurate spin-correlated decays on the differential distributions and found that leptonic observables are particularly sensitive to spin-correlation effects. Finally, we also quantified the impact of the $\mathcal{O}(\alpha_s \alpha^3)$ contributions at the differential level. For most observables these contributions amount to a flat +10% correction, while for a few observables sensitive to forward jets they can become more sizable.

It is interesting to notice that even though the on-shell modeling of $t\bar{t}W^{\pm}$ EW production largely depends on the matching and parton-shower settings of each generator, these effects are much less visible for full predictions once QCD and EW contributions are combined. Furthermore, giving the fact that the two same-sign lepton signature is dominated by jets emerging from a hadronic W decay that in all generators is modeled only at LO, for this particular signature it will be very important to improve on the

theoretical description of these jets in the future. With respect to this, the modeling of the two same-sign lepton signature could be improved by a fixed-order full off-shell computation similar to Ref. [82], as the corresponding matching to parton showers would be computationally challenging. The narrow-width approximation presents an alternative to include one-loop QCD corrections to the top-quark and W boson decays and could be included in an event generator, as has been already shown in Ref. [83]. On the other hand, other fiducial signatures, like the ones involving three leptons and no hadronic W decay, may require the inclusion of higher-order corrections [like $\mathcal{O}(\alpha_s^4 \alpha)$ NNLO corrections] to the production process to reach a better control of the corresponding theoretical systematics. In all cases the impact of radiative top-quark decays should be studied carefully. Finally, we want to emphasize the fact that even though for the current center-of-mass energy of the LHC of $\sqrt{s} = 13$ TeV the modeling of the subleading $\mathcal{O}(\alpha_s \alpha^3)$ contribution only plays a minor role at the fiducial level it will be crucial to improve on its theoretical accuracy for higher center-of-mass energies, as its radiative contribution will increase [12].

It is clear from our discussion that providing a robust theoretical prediction for hadronic $t\bar{t}W^{\pm}$ production cannot be framed as a unique recipe and care must be taken to analyze the specific characteristics of different observables measured in experiments. Having at our disposal several well-tested tools that allow us to implement state-of-the-art theoretical calculations in the modeling of collider events is clearly valuable and offers us the possibility of studying the problem in its complexity and identify where improvement is most needed.

The POWHEG event generator Wtt_dec is publicly available as part of the POWHEG-BOX repository [84].

APPENDIX: OFF-SHELL MOMENTUM MAPPING

In this section we elaborate on the momentum mapping between on-shell and off-shell momenta used in Sec. III B to include a smearing of the particle masses according to a Breit-Wigner distribution. The mapping discussed below is an adaptation of the method presented in Ref. [85], which itself was based on the momentum mapping of Ref. [86]. The momentum mapping is Lorentz invariant and preserves

the center-of-mass energy as well as the overall momentum of the momentum configuration. The mapping is constructed such that it generates a new off-shell momentum $\hat{p}_l$ with $\hat{p}_l^2 = v_l^2$ starting from an on-shell momentum p_l, with $p_l^2 = m_l^2$ by borrowing some of the necessary energy from the remaining recoiling final state. The new momentum $\hat{p}_l$ is parametrized by

$$\hat{p}_l = \lambda p_l + \frac{1 - \lambda + y}{2a_l} Q, \qquad \hat{p}_l^2 = v_l^2, \qquad (A1)$$

where Q is the total final state momentum and v_l^2 is the new virtuality of the off-shell momentum. Furthermore, we introduce the following dimensionless variables:

$$a_l = \frac{Q^2}{2(Q \cdot p_l)}, \qquad b_l = \frac{m_l^2}{2(Q \cdot p_l)}, \qquad c_l = \frac{v_l^2}{2(Q \cdot p_l)}. \qquad (A2)$$

The parameter λ can be determined by requiring that the invariant mass of the recoiling momenta before and after the mapping are preserved, which are given by

$$K = Q - p_l, \qquad K^2 = 2(Q \cdot p_l)[a_l + b_l - 1], \qquad \hat{K} = Q - \hat{p}_l,$$

$$\hat{K}^2 = \frac{2(Q \cdot p_l)}{4a_l}[(2a_l - 1 - y)^2 - (1 - 4a_l b_l)\lambda^2]. \qquad (A3)$$

Equating $K^2 = \hat{K}^2$ then yields

$$\lambda = \sqrt{\frac{(1 + y)^2 - 4a_l(y + b_l)}{1 - 4a_l b_l}}. \qquad (A4)$$

The remaining parameter y can be fixed from the condition

$$\hat{p}_l^2 = 2(Q \cdot p_l)(y + b_l) \overset{!}{=} v_l^2 = 2(Q \cdot p_l)c_l, \qquad (A5)$$

which defines y as a measure of the virtuality:

$$y = c_l - b_l = \frac{v_l^2 - m_l^2}{2(Q \cdot p_l)}. \qquad (A6)$$

The upper boundary on the virtuality is given by the value y_{max} for which λ vanishes and is given by

$$y_{max} = (\sqrt{a_l} - \sqrt{a_l + b_l - 1})^2 - b_l. \qquad (A7)$$

In order to preserve momentum conservation the recoiling momenta have to be boosted:

$$\hat{p}_i^\mu = \Lambda^\mu{}_\nu p_i^\nu, \qquad i \neq l, \qquad (A8)$$

with the Lorentz transformation

$$\Lambda^\mu{}_\nu = g^\mu{}_\nu - \frac{2(K + \hat{K})^\mu (K + \hat{K})_\nu}{(K + \hat{K})^2} + \frac{2\hat{K}^\mu K_\nu}{K^2}. \qquad (A9)$$

[1] F. Maltoni, M. L. Mangano, I. Tsinikos, and M. Zaro, Top-quark charge asymmetry and polarization in $t\bar{t}W^\pm$ production at the LHC, Phys. Lett. B **736**, 252 (2014).

[2] G. Bevilacqua, H.-Y. Bi, H. Bayu Hartanto, M. Kraus, J. Nasufi, and M. Worek, NLO QCD corrections to off-shell $t\bar{t}W^\pm$ production at the LHC: Correlations and asymmetries, arXiv:2012.01363.

[3] F. Maltoni, D. Pagani, and I. Tsinikos, Associated production of a top-quark pair with vector bosons at NLO in QCD: Impact on $t\bar{t}H$ searches at the LHC, J. High Energy Phys. 02 (2016) 113.

[4] A. M Sirunyan et al. (CMS Collaboration), Observation of ttH Production, Phys. Rev. Lett. **120**, 231801 (2018).

[5] M. Aaboud et al. (ATLAS Collaboration), Observation of Higgs boson production in association with a top quark pair at the LHC with the ATLAS detector, Phys. Lett. B **784**, 173 (2018).

[6] Analysis of $t\bar{t}H$ and $t\bar{t}W$ production in multilepton final states with the ATLAS detector, Technical Report No. AT-LAS-CONF-2019-045, CERN, Geneva, 2019.

[7] A. M. Sirunyan et al. (CMS Collaboration), Measurement of the Higgs boson production rate in association with top quarks in final states with electrons, muons, and hadronically decaying tau leptons at $\sqrt{s} = 13$ TeV, arXiv:2011.03652.

[8] A. M. Sirunyan et al. (CMS Collaboration), Search for production of four top quarks in final states with same-sign or multiple leptons in proton-proton collisions at $\sqrt{s} = 13$ TeV, Eur. Phys. J. C **80**, 75 (2020).

[9] G. Aad et al. (ATLAS Collaboration), Evidence for $t\bar{t}t\bar{t}$ production in the multilepton final state in proton–proton collisions at $\sqrt{s} = 13$ TeV with the ATLAS detector, Eur. Phys. J. C **80**, 1085 (2020).

[10] J. M. Campbell and R. K. Ellis, $t\bar{t}W^{+-}$ production and decay at NLO, J. High Energy Phys. 07 (2012) 052.

[11] S. Frixione, V. Hirschi, D. Pagani, H. S. Shao, and M. Zaro, Electroweak and QCD corrections to top-pair hadroproduction in association with heavy bosons, J. High Energy Phys. 06 (2015) 184.

[12] R. Frederix, D. Pagani, and M. Zaro, Large NLO corrections in $t\bar{t}W^\pm$ and $t\bar{t}t\bar{t}$ hadroproduction from supposedly subleading EW contributions, J. High Energy Phys. 02 (2018) 031.

[13] P. Nason, A new method for combining NLO QCD with shower Monte Carlo algorithms, J. High Energy Phys. 11 (2004) 040.

[14] S. Frixione, P. Nason, and C. Oleari, Matching NLO QCD computations with Parton Shower simulations: The POW-HEG method, J. High Energy Phys. 11 (2007) 070.

[15] M. V. Garzelli, A. Kardos, C. G. Papadopoulos, and Z. Trocsanyi, t $\bar{t}$ W^{+-} and t $\bar{t}$ Z Hadroproduction at NLO accuracy in QCD with parton shower and hadronization effects, J. High Energy Phys. 11 (2012) 056.

[16] S. Frixione and B. R. Webber, Matching NLO QCD computations and parton shower simulations, J. High Energy Phys. 06 (2002) 029.

[17] S. Frixione, P. Nason, and B. R. Webber, Matching NLO QCD and parton showers in heavy flavor production, J. High Energy Phys. 08 (**2003**) 007.

[18] J. Alwall, R. Frederix, S. Frixione, V. Hirschi, F. Maltoni, O. Mattelaer, H. S. Shao, T. Stelzer, P. Torrielli, and M. Zaro, The automated computation of tree-level and next-to-leading order differential cross sections, and their matching to parton shower simulations, J. High Energy Phys. 07 (2014) 079.

[19] T. Gleisberg, S. Hoeche, F. Krauss, M. Schonherr, S. Schumann, F. Siegert, and J. Winter, Event generation with Sherpa 1.1, J. High Energy Phys. 02 (2009) 007.

[20] E. Bothmann et al. (Sherpa Collaboration), Event generation with Sherpa 2.2, SciPost Phys. **7,** 034 (2019).

[21] F. Cascioli, P. Maierhofer, and S. Pozzorini, Scattering Amplitudes with Open Loops, Phys. Rev. Lett. **108,** 111601 (2012).

[22] F. Buccioni, S. Pozzorini, and M. Zoller, On-the-fly reduction of Open Loops, Eur. Phys. J. C **78,** 70 (2018).

[23] F. Buccioni, J.-N. Lang, J. M. Lindert, P. Maierhöfer, S. Pozzorini, H. Zhang, and M. F. Zoller, OpenLoops 2, Eur. Phys. J. C **79,** 866 (2019).

[24] D. de Florian et al. (LHC Higgs Cross Section Working Group), Handbook of LHC Higgs cross sections: 4. Deciphering the nature of the Higgs sector, **2/2017** (2016), https://doi.org/10.23731/CYRM-2017-002 .

[25] H. T. Li, C. S. Li, and S. A. Li, Renormalization group improved predictions for $t\bar{t}W^{\pm}$ production at hadron colliders, Phys. Rev. D **90,** 094009 (2014).

[26] A. Broggio, A. Ferroglia, G. Ossola, and B. D. Pecjak, Associated production of a top pair and a W boson at next-to-next-to-leading logarithmic accuracy, J. High Energy Phys. 09 (2016) 089.

[27] A. Kulesza, L. Motyka, D. Schwartländer, T. Stebel, and V. Theeuwes, Associated production of a top quark pair with a heavy electroweak gauge boson at NLO + NNLL accuracy, Eur. Phys. J. C **79,** 249 (2019).

[28] A. Broggio, A. Ferroglia, R. Frederix, D. Pagani, B. D. Pecjak, and I. Tsinikos, Top-quark pair hadroproduction in association with a heavy boson at NLO + NNLL including EW corrections, J. High Energy Phys. 08 (2019) 039.

[29] A. Kulesza, L. Motyka, D. Schwartländer, T. Stebel, and V. Theeuwes, Associated top quark pair production with a heavy boson: Differential cross sections at NLO + NNLL accuracy, Eur. Phys. J. C **80,** 428 (2020).

[30] A. M. Sirunyan et al. (CMS Collaboration), Measurement of the cross section for top quark pair production in association with a W or Z boson in proton-proton collisions at $\sqrt{s}$ = 13 TeV, J. High Energy Phys. 08 (2018) 011.

[31] M. Aaboud et al. (ATLAS Collaboration), Measurement of the $t\bar{t}Z$ and $t\bar{t}W$ cross sections in proton-proton collisions at $\sqrt{s}$ = 13 TeV with the ATLAS detector, Phys. Rev. D **99,** 072009 (2019).

[32] G. Bevilacqua, H.-Y. Bi, H. B. Hartanto, M. Kraus, and M. Worek, The simplest of them all: $t\bar{t}W^{\pm}$ at NLO accuracy in QCD, J. High Energy Phys. 08 (2020) 043.

[33] A. Denner and G. Pelliccioli, NLO QCD corrections to off-shell t$\bar{t}$W$^+$ production at the LHC, J. High Energy Phys. 11 (2020) 069.

[34] R. Frederix and I. Tsinikos, Subleading EW corrections and spin-correlation effects in $t\bar{t}W$ multi-lepton signatures, Eur. Phys. J. C **80,** 803 (2020).

[35] S. von Buddenbrock, R. Ruiz, and B. Mellado, Anatomy of inclusive $t\bar{t}W$ production at hadron colliders, Phys. Lett. B **811,** 135964 (2020).

[36] Modelling of rare top quark processes at $\sqrt{s}$ = 13 TeV in ATLAS, Technical Report No. ATL-PHYS-PUB-2020-024, CERN, Geneva, 2020.

[37] S. Alioli, P. Nason, C. Oleari, and E. Re, A general framework for implementing NLO calculations in shower Monte Carlo programs: The POWHEG BOX, J. High Energy Phys. 06 (2010) 043.

[38] T. Sjostrand, S. Mrenna, and P. Z. Skands, PYTHIA 6.4 physics and manual, J. High Energy Phys. 05 (2006) 026.

[39] T. Sjöstrand, S. Ask, J. R. Christiansen, R. Corke, N. Desai, P. Ilten, S. Mrenna, S. Prestel, C. O. Rasmussen, and P. Z. Skands, An introduction to PYTHIA 8.2, Comput. Phys. Commun. **191,** 159 (2015).

[40] S. Schumann and F. Krauss, A parton shower algorithm based on Catani-Seymour dipole factorisation, J. High Energy Phys. 03 (2008) 038.

[41] S. Alioli, P. Nason, C. Oleari, and E. Re, NLO Higgs boson production via gluon fusion matched with shower in POWHEG, J. High Energy Phys. 04 (2009) 002.

[42] S. Alioli, P. Nason, C. Oleari, and E. Re, NLO vector-boson production matched with shower in POWHEG, J. High Energy Phys. 07 (2008) 060.

[43] J. A. Dror, M. Farina, E. Salvioni, and J. Serra, Strong tW scattering at the LHC, J. High Energy Phys. 01 (2016) 071.

[44] T. Stelzer and W. F. Long, Automatic generation of tree level helicity amplitudes, Comput. Phys. Commun. **81,** 357 (1994).

[45] J. Alwall, P. Demin, S. de Visscher, R. Frederix, M. Herquet, F. Maltoni, T. Plehn, D. L. Rainwater, and T. Stelzer, MadGraph/MadEvent v4: The new web generation, J. High Energy Phys. 09 (2007) 028.

[46] S. Honeywell, S. Quackenbush, L. Reina, and C. Reuschle, NLOX, a one-loop provider for Standard Model processes, Comput. Phys. Commun. **257,** 107284 (2020).

[47] D. Figueroa, S. Quackenbush, L. Reina, and C. Reuschle, Updates to the one-loop provider NLOX, arXiv:2101.01305.

[48] A. van Hameren, OneLOop: For the evaluation of one-loop scalar functions, Comput. Phys. Commun. **182,** 2427 (2011).

[49] H. B. Hartanto, B. Jager, L. Reina, and D. Wackeroth, Higgs boson production in association with top quarks in the POWHEG BOX, Phys. Rev. D **91,** 094003 (2015).

[50] S. Actis, A. Denner, L. Hofer, A. Scharf, and S. Uccirati, Recursive generation of one-loop amplitudes in the Standard Model, J. High Energy Phys. 04 (2013) 037.

[51] S. Actis, A. Denner, L. Hofer, J.-N. Lang, A. Scharf, and S. Uccirati, RECOLA: REcursive Computation of One-Loop Amplitudes, Comput. Phys. Commun. **214,** 140 (2017).

[52] J. Alwall, M. Herquet, F. Maltoni, O. Mattelaer, and T. Stelzer, MadGraph 5: Going beyond, J. High Energy Phys. 06 (2011) 128.

[53] F. R. Anger, F. F. Cordero, H. Ita, and V. Sotnikov, NLO QCD predictions for $Wb\bar{b}$ production in association with up to three light jets at the LHC, Phys. Rev. D **97,** 036018 (2018).

[54] C. Oleari and L. Reina, W + − b $\bar{b}$ production in POWHEG, J. High Energy Phys. 08 (2011) 061; 11 (2011) 040(E).

[55] E. Boos et al., Generic user process interface for event generators, in Proceedings of the 2nd Les Houches Workshop on Physics at TeV Colliders (2001) [arXiv: hep-ph/0109068].

[56] J. Alwall et al., A Standard format for Les Houches event files, Comput. Phys. Commun. **176,** 300 (2007).

[57] S. Frixione, E. Laenen, P. Motylinski, and B. R. Webber, Angular correlations of lepton pairs from vector boson and top quark decays in Monte Carlo simulations, J. High Energy Phys. 04 (2007) 081.

[58] S. Alioli, P. Nason, C. Oleari, and E. Re, NLO single-top production matched with shower in POWHEG: s- and t-channel contributions, J. High Energy Phys. 09 (2009) 011(E); 02 (2010) 11.

[59] S. Alioli, S.-O. Moch, and P. Uwer, Hadronic top-quark pair-production with one jet and parton showering, J. High Energy Phys. 01 (2012) 137.

[60] P. Artoisenet, R. Frederix, O. Mattelaer, and R. Rietkerk, Automatic spin-entangled decays of heavy resonances in Monte Carlo simulations, J. High Energy Phys. 03 (2013) 015.

[61] R. D. Ball et al. (NNPDF Collaboration), Parton distributions for the LHC Run II, J. High Energy Phys. 04 (2015) 040.

[62] A. Buckley, J. Ferrando, S. Lloyd, K. Nordström, B. Page, M. Rüfenacht, M. Schönherr, and G. Watt, LHAPDF6: Parton density access in the LHC precision era, Eur. Phys. J. C **75,** 132 (2015).

[63] S. Catani, F. Krauss, R. Kuhn, and B. R. Webber, QCD matrix elements + parton showers, J. High Energy Phys. 11 (2001) 063.

[64] S. Hoeche, F. Krauss, S. Schumann, and F. Siegert, QCD matrix elements and truncated showers, J. High Energy Phys. 05 (2009) 053.

[65] P. Richardson, Spin correlations in Monte Carlo simulations, J. High Energy Phys. 11 (2001) 029.

[66] M. Dobbs and J. B. Hansen, The HepMC C++ Monte Carlo event record for high energy physics, Technical Report No. ATL-SOFT-2000-001 (CERN, Geneva, 2000) revised version number 1 submitted on 2001-02-27, 09:54:32.

[67] A. Buckley, P. Ilten, D. Konstantinov, L. Lönnblad, J. Monk, W. Porkorski, T. Przedzinski, and A. Verbytskyi, The HepMC3 event record library for Monte Carlo event generators, Comput. Phys. Commun. **260,** 107310 (2021).

[68] A. Buckley, J. Butterworth, L. Lonnblad, D. Grellscheid, H. Hoeth, J. Monk, H. Schulz, and F. Siegert, Rivet user manual, Comput. Phys. Commun. **184,** 2803 (2013).

[69] C. Bierlich et al., Robust independent validation of experiment and theory: Rivet version 3, SciPost Phys. **8,** 026 (2020).

[70] See Supplemental Material at http://link.aps.org/supplemental/10.1103/PhysRevD.103.094014 for reproducibility we provide input run cards for the POWHEG-BOX and Sherpa as well as the Rivet analysis files for our presented studies.

[71] M. Cacciari, G. P. Salam, and G. Soyez, The anti-k_t jet clustering algorithm, J. High Energy Phys. 04 (2008) 063.

[72] M. Cacciari and G. P. Salam, Dispelling the N^3 myth for the k_t jet-finder, Phys. Lett. B **641,** 57 (2006).

[73] M. Cacciari, G. P. Salam, and G. Soyez, FastJet user manual, Eur. Phys. J. C **72,** 1896 (2012).

[74] D. L. Rainwater, R. Szalapski, and D. Zeppenfeld, Probing color singlet exchange in Z + two jet events at the CERN LHC, Phys. Rev. D **54,** 6680 (1996).

[75] T. Ježo, J. M. Lindert, P. Nason, C. Oleari, and S. Pozzorini, An NLO + PS generator for $t\bar{t}$ and Wt production and decay including non-resonant and interference effects, Eur. Phys. J. C **76,** 691 (2016).

[76] I. I. Y. Bigi, Y. L. Dokshitzer, V. A. Khoze, J. H. Kuhn, and P. M. Zerwas, Production and Decay Properties of Ultra-heavy Quarks, Phys. Lett. B **181,** 157 (1986).

[77] V. D. Barger, J. Ohnemus, and R. J. N. Phillips, Spin correlation effects in the hadroproduction and decay of very heavy top quark pairs, Int. J. Mod. Phys. A **04,** 617 (1989).

[78] W. Bernreuther, A. Brandenburg, and P. Uwer, Transverse polarization of top quark pairs at the Tevatron and the large hadron collider, Phys. Lett. B **368,** 153 (1996).

[79] G. Mahlon and S. J. Parke, Angular correlations in top quark pair production and decay at hadron colliders, Phys. Rev. D **53,** 4886 (1996).

[80] A. Behring, M. Czakon, A. Mitov, A. S. Papanastasiou, and R. Poncelet, Higher Order Corrections to Spin Correlations In Top Quark Pair Production at the LHC, Phys. Rev. Lett. **123,** 082001 (2019).

[81] M. Czakon, A. Mitov, and R. Poncelet, NNLO QCD corrections to leptonic observables in top-quark pair production and decay, arXiv:2008.11133.

[82] A. Denner and M. Pellen, Off-shell production of top-antitop pairs in the lepton + jets channel at NLO QCD, J. High Energy Phys. 02 (**2018**) 013.

[83] J. M. Campbell, R. K. Ellis, P. Nason, and E. Re, Top-pair production and decay at NLO matched with parton showers, J. High Energy Phys. 04 (2015) 114.

[84] http://powhegbox.mib.infn.it.

[85] M. Czakon, H. B. Hartanto, M. Kraus, and M. Worek, Matching the Nagy-Soper parton shower at next-to-leading order, J. High Energy Phys. 06 (2015) 033.

[86] Z. Nagy and D. E. Soper, Parton showers with quantum interference, J. High Energy Phys. 09 (2007) 114.